Anisotropic compact stars in the Buchdahl model: A comprehensive study

S. K. Maurya[*]
Department of Mathematical and Physical Sciences, College of Arts and Science, University of Nizwa, Nizwa, Sultanate of Oman

Ayan Banerjee[†]
Astrophysics and Cosmology Research Unit, University of KwaZulu Natal, Private Bag X54001, Durban 4000, South Africa

M. K. Jasim[‡]
Department of Mathematical and Physical Sciences, University of Nizwa, Nizwa 616, Sultanate of Oman

J. Kumar and A. K. Prasad[§]
Department of Applied Mathematics, Central University of Jharkhand, Ranchi 835205, India

Anirudh Pradhan[‖]
Department of Mathematics, Institute of Applied Sciences & Humanities, GLA University, Mathura 281 406, Uttar Pradesh, India

(Received 24 November 2018; published 15 February 2019)

In this article we present a class of relativistic solutions describing spherically symmetric and static anisotropic stars in hydrostatic equilibrium. For this purpose, we consider a particularized metric potential, namely, Buchdahl ansatz [Phys. Rev. D **116**, 1027 (1959).] which encompasses almost all the known analytic solutions to the spherically symmetric, static Einstein equations with a perfect fluid source, including, in particular, the Vaidya-Tikekar and Finch-Skea. We developed the model by considering an anisotropic spherically symmetric static general relativistic configuration that has a significant effect on the structure and properties of stellar objects. We have considered eight different cases for generalized Buchdahl dimensionless parameter K and analyzed them in a uniform manner. As a result it turns out that all the considered cases are valid at every point in the interior spacetime. In addition to this, we show that the model satisfies all the energy conditions and maintains the hydrostatic equilibrium equation. In the frame work of anisotropic hypothesis, we consider analogue objects with similar mass and radii, such as LMC X-4, SMC X-1, EXO 1785-248 etc. to restrict the model parameter arbitrariness. Also, establishing a relation between pressure and density in the form of $P = P(\rho)$, we demonstrate that equation of state (EoS) can be approximated to a linear function of density. Despite the simplicity of this model, the obtained results are satisfactory.

DOI: 10.1103/PhysRevD.99.044029

I. INTRODUCTION

In astrophysics, studying the structural properties and formation of compact objects, such as neutron stars (NSs) and quark stars (QSs), has attracted much attention to the researchers in the context of General Relativity (GR), as well as widely developing modified theories of gravity. Crudely, compact stars are the final stages in the evolution of ordinary stars which become an excellent test bed for the study of highly dense matter in extreme conditions. In recent times, a number of compact objects with high densities have been discovered [1], which are often observed as pulsars, spinning stars with strong magnetic fields. Our theoretical understanding about compact stars is rooted in the Fermi-Dirac statistics, which are responsible for the high degeneracy pressure that holds up the star against gravitational collapse and was proposed by Fowler in 1926 [2]. Shortly afterwards, using Einstein's special theory of relativity and the principles of quantum physics, Chandrasekhar showed that [3,4] white dwarfs are compact stars, which are supported solely by a degenerate gas of electrons, to be stable if the maximum size of a stable white dwarf is approximately 3×10^{30} kg (about 1.4 times the mass of the Sun).

[*]sunil@unizwa.edu.om
[†]ayan_7575@yahoo.co.in
[‡]mahmoodkhalid@unizwa.edu.om
[§]jitendark@gmail.com
[‖]pradhan.anirudh@gmail.com

As of today, there is no comprehensive description of extremely dense matter in a strongly interacting regime. A possible theoretical description of such nuclear matter in extreme densities may consist not only of leptons and nucleons but also several exotic components in their different forms and phases such as hyperons, mesons, baryon resonances, as well as strange quark matter (SQM). Therefore, a real composition of matter distribution in the interior of compact objects remains a question for deeper examination. The most general spherically symmetric matter distribution is usually thought to be an isotropic fluid, because astrophysical observations support isotropy. A possible theoretical algorithm was proposed by Fodor [5] that can generate any number of physically realistic pressure and density profiles for isotropic distributions without evaluating integrals.

On one hand, when densities of compact objects are normally above the nuclear matter density, one can expect the appearance of unequal principal stresses, the so-called anisotropic fluid. This usually means that two different kinds of pressures inside these compact objects, viz., the radial pressure and the tangential pressure [6]. This leads to the anisotropic condition that the radial pressure component, p_r is not equal to the components in the transverse direction, p_t. This effect was first predicted in 1922 by J. H. Jeans [7] for self-gravitating objects in the Newtonian regime. Shortly later, in the context of GR, Lemaître [8] had also considered the local anisotropy effect and showed that one can relax the upper limits imposed on the maximum value of the surface gravitational potential. Ruderman [9] gave an interesting picture about more realistic stellar models and showed that a star with matter density ($\rho > 10^{15}$ gm/cm^3), where the nuclear interaction becomes relativistic in nature, is likely to be anisotropic.

The inclusion of anisotropic effects on compact objects was first considered by Bowers and Liang [10] in 1974. They studied static spherically symmetric configurations and analyzed the hydrostatic equilibrium equation, modified from of its original form to include the anisotropy effects. Moreover, they provided the results by making a comparison with the stars filled with isotropic fluid. Heintzmann and Hillebrandt [11] have investigated neutron star models at high densities with an anisotropic equation of state and found for arbitrary large anisotropy there is no limiting mass for neutron stars, though the maximum mass of a neutron star still lies beyond 3–4 $M_\odot$. A lot of works have been carried out in deriving new physical solutions with interior anisotropic fluids. Herrera and Santos [6] reviewed and discussed possible causes for the appearance of local anisotropy in self gravitating systems with examples of both Newtonian and general relativistic contexts. In [12], a class of exact solutions of Einstein's gravitational field equations have been put forward for the existence of anisotropy in star models. In addition, Harko and his collaborators [13–17] have done some significant work on anisotropic matter distribution. For new exact interior solutions to the Einstein field equations, Chaisi and Maharaj [18] have studied the gravitational behavior of compact objects under strong gravitational fields. Very recently, an analysis based on the linear quark equation of state (EoS) for finding the equilibrium conditions of an anisotropically sustained charged spherical body has been revisited by Sunzu *et al.* [19]. The studies developed in [20–25] form part of a quantity of works where the influence of the anisotropic effect on the structure of static spherically symmetric compact objects is analyzed. In favor of anisotropy, Kalam *et al.* [26] have developed a star model and showed that central density depends on the anisotropic factor. For recent investigations, there have been important efforts in describing the relativistic stellar structure in [27–30]. The algorithm for solutions of Einstein field equations via single monotone functions have already been discovered by the authors of [31–33].

On the other hand, spherical symmetry also allows a more general anisotropic fluid configuration with an EoS. In fact, if the EoS of the material composition of a compact star is known, one can easily integrate the Tolman-Oppenheimer-Volkoff (TOV) equations to extract the geometrical information of a star. For example, linear EoS was used by Ivanov [34] for charged static spherically symmetric perfect fluid solutions. This situation has been extended by Sharma and Maharaj [35] for finding an exact solution to the Einstein field equations with an anisotropic matter distribution. In Ref. [36], Herrera and Barreto had considered polytropic stars with anisotropic pressure. Solutions of Einstein's equations for anisotropic fluid distribution with different EoS have been found in [24,37–41], but, in case the EoS of the material composition of a compact star is not yet known, except some phenomenological assumptions, one can introduce a suitable metric ansatz for one of the metric functions to analyze the physical features of the star. Such a method was initially proposed by Vaidya-Tikekar [42], and Tikekar [43] prescribed an approach of assigning different geometries with physical 3-spaces (see [44–47] and references therein). A similar type of metric ansatz was considered by Finch and Skea [48] satisfying all criteria of physical acceptability according to Delgaty and Lake [49]. As a consequence,the problem of finding the equilibrium configuration of a stellar structure for anisotropic fluid distribution has been found in [50–53].

In the present paper, we consider fairly general Buchdahl ansatz [54] for the metric potential. Such an assumption makes Einstein's field equations tractable and covers almost all physically tenable known models of super dense stars. Actually, Vaidya and Tikekar [42] particularized a Buchdahl ansatz by giving a geometric meaning, prescribing specific 3-spheroidal geometries for a 4-dimensional hypersurface. This spheroidal condition has been found very useful for finding an exact solution of the Einstein

field equations, which is not easy in many other cases. Such a particular assumption was considered by Kumar *et al.* [55,56], who comprehensively studied charged compact objects for isotropic matter distribution. Sharma *et al.* [57] have obtained the maximum possible masses and radii for different values of surface density for Vaidya-Tikekar spacetime.

Neutron stars, the remnants of the gravitational collapse of ∼8 to 20 $M_\odot$ main-sequence stars, in which fundamental physics can be probed in extreme conditions via astrophysical observations. The structure of such stars depends on the EoS of nuclear matter under extreme conditions. Thus, neutron stars are an excellent probe for the study of dense and strongly interacting matter. More specifically, the mass-radius of a neutron star is directly related to the EoS of neutron-rich matter [58], and this could be achieved through the independent measurement of its mass and radius [59–62].

From an observational viewpoint, our understanding about neutron stars has changed drastically in the last decade after the discovery of pulsar PSR J1614-2230 [63] as 1.97 $M_\odot$. The most significant progress in determining the properties of neutron stars, such as their masses and radii, which is necessary for constraining the equation of state. However, obtaining accurate measurements of both the mass and radius of neutron stars is more difficult. To date, only in a few cases have the mass and radius of compact stars been estimated by exploiting a variety of observational techniques, including, in particular, radio observations of pulsars and X-ray spectroscopy, for example, during thermonuclear bursts [64–66] or in the quiescent state of low mass X-ray binaries [67,68]. It is therefore greatly important to understand the maximal mass value of such objects which is still an open question, but recent observations estimate this limit as ∼2 $M_\odot$, while, for the pulsar J0348 + 0432, it is 2.01 $M_\odot$ [69]. Recent studies have reported massive neutron stars to be PSR J1614 + 2230 (∼1.97 $M_\odot$ [63]), Vela X-1 (∼1.8 $M_\odot$ [70]), and 4U 1822-371 (∼2 $M_\odot$ [71]). X-ray pulsations with a period of 13.5 s were first detected in LMC X-4 by Kelley *et al.* [72]. However, the maximal limit of neutron star mass can increase considerably due to strong magnetic fields inside the star.

Thus, neutron stars are very peculiar objects, and observational data about their macroscopic properties (mainly the mass-radius M-R relation) can also be used for studying accurate derivations consistent with the observations. In this paper, we discuss the possibility of an extendable range of the Buchdahl dimensionless parameter K (a measure of deviation from sphericity) to explore a class of neutron stars in the standard framework of General Relativity. In our model, we do not prescribe the EoS; rather we apply the two-step method to examine the possibility of using the anisotropy to obtain spherically symmetric configurations with the Buchdahl metric potential. In order to constrain the value of model parameters, we consider analogue objects with similar mass and radii, such as LMC X-4 [72], SMC X-1 [70], EXO 1785-248 [73], SAX J1808.4-3658 (SS2) [74], Her X-1 [75], 4U 1538-52 [70], PSR 1937 + 21 [76], and Cen X-3 [70] to those stars in Buchdahl anisotropic geometry.

The paper begins with the introduction in Sec. I, then we introduce the relevant Einstein equations for the case of spherical symmetry static spacetime in the standard form of Schwarzschild-like coordinates in Sec. II. In Sec. III, we assume anisotropic pressure in the modeling of realistic compact stellar structures. In the same section we derive the field equations by using coordinate transformation and found eight possible solutions for positive and negative values of Buchdahl parameter K. In Sec. IV, we discuss the junction conditions and determine the constant coefficient. We also presented the mass-radius relation and surface redshift of the stellar models in same section. Section V includes detailed analysis of physical features and obtained results are compared with data from observation along with the equation of state (EoS) of the compact star. Concluding remarks have been made in Sec. VI.

II. GENERAL RELATIVISTIC EQUATIONS

Let us consider the spacetime being static and spherically symmetric, which describes the interior of the object, and can be written in the following form:

$$ds^2 = -e^{\nu(r)}dt^2 + e^{\lambda(r)}dr^2 + r^2(d\theta^2 + \sin^2\theta d\phi^2), \quad (1)$$

where the coordinates (t, r, θ, ϕ) are the Schwarzschild-like coordinates, and $\nu(r)$ and $\lambda(r)$ are arbitrary functions of the radial coordinate r alone, which are yet to be determined. The Einstein tensor is $G_{\mu\nu} = R_{\mu\nu} - \frac{1}{2}g_{\mu\nu}R$, with $R_{\mu\nu}$ and $g_{\mu\nu}$ being, respectively, the Ricci and the metric tensors, and R being the Ricci scalar (with the assumption of natural units $G = c = 1$).

Here, we consider the matter contained in the sphere which is described by anisotropic fluid. Thus, the structure of such an energy-momentum tensor is then expected to be of the form:

$$T_{\mu\nu} = (\rho + p_t)u_\mu u_\nu - p_t g_{\mu\nu} + (p_r - p_t)\chi^\mu\chi_\nu, \quad (2)$$

where u_μ is the four-velocity and χ_μ is the unit spacelike vector in the radial direction. Thus, the Einstein field equation, $G_{\mu\nu} = 8\pi T_{\mu\nu}$, provides the following set of gravitational field equations:

$$\kappa\rho(r) = \frac{\lambda'}{r}e^{-\lambda} + \frac{(1 - e^{-\lambda})}{r^2}, \quad (3)$$

$$\kappa p_r(r) = \frac{\nu'}{r}e^{-\lambda} - \frac{(1 - e^{-\lambda})}{r^2}, \quad (4)$$

$$\kappa p_t(r) = e^{-\lambda}\left[\frac{\nu''}{2} - \frac{\lambda'\nu'}{4} + \frac{\nu'^2}{4} + \frac{\nu' - \lambda'}{2r}\right], \tag{5}$$

where the prime denotes a derivative with respect to the radial coordinate, r, and $\kappa = 8\pi$. Here, ρ is the energy density, while the quantity p_r is the pressure in the direction of χ^ν (radial pressure), and p_t is the pressure orthogonal to χ_ν (transversal pressure). Note that pressure isotropy is not required by spherical symmetry, it is an added assumption [12,77]. Consequently, $\Delta = p_t - p_r$ is denoted as the anisotropy factor according to Herrera and Leon [78], and it measures the pressure anisotropy of the fluid. It is to be noted that at the origin of the stellar configuration $\Delta = 0$, i.e., $p_t = p_r = p$ is a particular case of an isotropic pressure. Using Eqs. (4) and (5), one can obtain the simple form of anisotropic factor, which yields

$$\Delta = \kappa(p_t - p_r) = e^{-\lambda}\left[\frac{\nu''}{2} - \frac{\lambda'\nu'}{4} + \frac{\nu'^2}{4} - \frac{\nu' + \lambda'}{2r} - \frac{1}{r^2}\right] + \frac{1}{r^2}. \tag{6}$$

However, a force due to the anisotropic pressure is represented by Δ/r, which is repulsive if $p_t > p_r$, and attractive if $p_t < p_r$ of the stellar model. For the considered matter distribution when $p_t > p_r$ allows the construction of more compact objects, compared to isotropic fluid sphere [79]. Note that this is a system of 3 equations with 5 unknowns. Thus, the system of equations is undetermined, and by assuming suitable conditions we have to reduce the number of unknown functions.

III. EXACT SOLUTION OF THE MODELS FOR ANISOTROPIC STARS

In this section we establish a procedure for generating a new anisotropic solution of the Einstein field equations from a known metric ansatz due to Buchdahl [54] that covers almost all interesting solutions. We use the widely studied metric ansatz given by

$$e^{\lambda} = \frac{K(1 + Cr^2)}{K + Cr^2}, \quad \text{when } K < 0 \quad \text{and} \quad K > 1, \tag{7}$$

where K and C are two parameters that characterize the geometry of the star. Note that the ansatz for the metric function g_{rr} in (7) was proposed by Buchdahl [54] to develop a viable model for a relativistic compact star. The choice of the metric potential is physically well motivated (especially as the energy density must be nonsingular and decreasing outward) and has been used by many in the past to construct viable stellar models. In addition to the above the metric function (7) is also positive and free from singularity at $r = 0$ and monotonic increasing outward. Here, we will illustrate how an analytic Buchdahl model could be extendable for positive and negative values of the spheroidal parameter K. In the following analysis we pull out the range of $0 < K < 1$, where either the energy density or pressure will be negative depending on the two parameters. It is interesting to note that one can recover the Schwarzschild interior solution when $K = 0$, and for $K = 1$ the hypersurfaces $\{t = \text{constant}\}$ are flat. In a more generic situation, one could recover the Vaidya and Tikekar [42] solution when $C = -K/R^2$, Durgapal and Bannerji [80] when $K = -2$. The solutions for charged and uncharged perfect fluids were considered by Gupta *et al.* [81,82], but none of them were well behaved within the proposed range of parameter K. However, in the present study we obtain the well behaved solution for some values of K by introducing anisotropy parameter Δ, which provides a monotonically decreasing sound speed within the compact stellar model.

As a next step in our analysis we introduce the transformation $e^{\nu} = Y^2(r)$ [34,55,56], and substituting the value of e^{λ} into the Eq. (6), one arrives in the following relations:

$$\frac{d^2Y}{dr^2} - \left[\frac{K + 2KCr^2 + C^2r^4}{r(K + Cr^2)(1 + Cr^2)}\right]\frac{dY}{dr} + \left[\frac{C(1 - K)C^2r^4}{r^2(K + Cr^2)(1 + Cr^2)} - \frac{\Delta K(1 + Cr^2)}{(K + Cr^2)}\right]Y = 0. \tag{8}$$

Eq. (8) has two unknowns, namely, $Y(r)$ and Δ, while in order to solve for Y, we will follow the approach in [12]. Hence, we choose the expressions for anisotropy parameter $\Delta = \frac{\Delta_0 C^2 r^2}{(1+Cr^2)^2}$. The constant $\Delta_0 \geq 0$, with the assumption that $\Delta_0 = 0$, corresponding to the isotropic limit. As argued in [12], Δ_0 is the measure of anisotropy of the pressure distribution inside the fluid sphere, while at the center the anisotropy vanishes, i.e., $\Delta(0) = 0$. With hindsight, for the chosen anisotropy parameter the interior solutions ensure the regularity condition at the center also.

Therefore, with this choice of Δ and using an appropriate transformation $Z = \sqrt{\frac{K+Cr^2}{K-1}}$, Eq. (8) becomes a hypergeometric differential equation of the form:

$$(1 - Z^2)\frac{d^2Y}{dZ^2} + Z\frac{dY}{dZ} + (1 - K + \Delta_0 K)Y = 0. \tag{9}$$

Our aim here is to solve the system of the above hypergeometric Eq. (9) by using Gupta-Jasim [82] two-step method (See Appendix A.). In this framework we consider two cases for the spheroidal parameter K:

A. Case I: $K < 0$, i.e., K is negative

Now we differentiate Eq. (9) with respect to Z and use another substitution, where $Z = \sin x$ and $\frac{dY}{dZ} = \psi$; then we have

$$\frac{d^2\psi}{dx^2} + (2 - K + \Delta_0 K)\psi = 0, \tag{10}$$

where $\frac{d\psi}{dx} = \cos x \frac{d^2Y}{dZ^2}$ and $\frac{d^2\psi}{dx^2} = \cos^2 x \frac{d^3Y}{dZ^3} - \sin x \frac{d^2Y}{dZ^2}$, respectively. In this approach the above equation turns out to be a second order homogeneous differential equation with constant coefficients and depends on the two parameters K and Δ_0. It is now interesting to classify each solution of Eq. (10), briefly:

$$\text{Case Ia: } \psi = A_1 \cosh(nx) + B_1 \sinh(nx), \qquad \text{if } 2 - K + \Delta_0 K = -n^2, \tag{11a}$$

$$\text{Case Ib: } \psi = C_1 \cos(nx) + D_1 \sin(nx), \qquad \text{if } 2 - K + \Delta_0 K = n^2 (\neq 1), \tag{11b}$$

$$\text{Case Ic: } \psi = E_1 \cos(x) + F_1 \sin(x), \qquad \text{if } 2 - K + \Delta_0 K = 1, \tag{11c}$$

$$\text{Case Id: } \psi = G_1 x + H_1, \qquad \text{if } 2 - K + \Delta_0 K = 0, \tag{11d}$$

where A_1, B_1, C_1, D_1, E_1, F_1, G_1, and H_1 are arbitrary constants of integration, with $x = \sin^{-1} Z = \sin^{-1} \sqrt{\frac{K+Cr^2}{K-1}}$. Now, using (7) into (3) from which simple manipulations of the Einstein equations lead to the expression of energy density ($K < 0$) as

$$\frac{\kappa\rho}{C} = \frac{(3 - K + K\sin^2 x - \sin^2 x)}{K(K-1)\cos^4 x}. \tag{12}$$

Subsequently, other Einstein field equations (EFEs) relating to the metric potential and substituting different values of Y [which is determined by substituting $dY/dZ = \psi$ and $d^2Y/dZ^2 = d\psi/dZ$ in hypergeometric equation Eq. (9)], one can obtain

Case Ia: $2 - K + \Delta_0 K = -n^2$

$$Y(x) = \frac{1}{(n^2+1)} [\cosh(nx)(A_1 \sin x + B_1 n \cos x) + \sinh(nx)(A_1 n \cos x + B_1 \sin x)], \tag{13}$$

$$\frac{\kappa p_r}{C} = \frac{2(n^2+1)}{(1-K)K\cos^2 x} \left[\frac{A_1 \cosh(nx) + B_1 \sinh(nx)}{\cosh(nx)(A_1 + B_1 n \cot x) + \sinh(nx)(A_1 n \cot x + B_1)}\right] + \frac{1}{K\cos^2 x}, \tag{14}$$

$$\frac{\kappa p_t}{C} = \frac{2(n^2+1)}{(1-K)K\cos^2 x} \left[\frac{A_1 \cosh(nx) + B_1 \sinh(nx)}{\cosh(nx)(A_1 + B_1 n \cot x) + \sinh(nx)(A_1 n \cot x + B_1)}\right] + \Upsilon. \tag{15}$$

Case Ib: $2 - K + \Delta_0 K = n^2 (\neq 1)$

$$Y(x) = \frac{1}{(1-n^2)} [\sin x [C_1 \cos(nx) + D_1 \sin(nx) - n \cos x [C_1 \sin(nx) - D_1 \cos(nx)]], \tag{16}$$

$$\frac{\kappa p_r}{C} = \frac{2(1-n^2)}{(1-K)K\cos^2 x} \left[\frac{C_1 \cos(nx) + D_1 \sin(nx)}{C_1 \cos(nx) + D_1 \sin(nx) - n \cot x [C_1 \sin(nx) - D_1 \cos(nx)}\right] + \frac{1}{K\cos^2 x}, \tag{17}$$

$$\frac{\kappa p_t}{C} = \frac{2(1-n^2)}{(1-K)K\cos^2 x} \left[\frac{C_1 \cos(nx) + D_1 \sin(nx)}{C_1 \cos(nx) + D_1 \sin(nx) - n \cot x [C_1 \sin(nx) - D_1 \cos(nx)}\right] + \Upsilon. \tag{18}$$

Case Ic: $2 - K + \Delta_0 K = 1$

$$Y(x) = \frac{1}{4} [E_1 (2x + \sin 2x) - F_1 \cos 2x], \tag{19}$$

$$\frac{\kappa p_r}{C} = \frac{8 \sin x}{(1-K)K\cos^2 x} \left[\frac{E_1 \cos(x) + F_1 \sin(x)}{E_1 (2x + \sin 2x) - F_1 \cos 2x}\right] + \frac{1}{K\cos^2 x}, \tag{20}$$

$$\frac{\kappa p_t}{C} = \frac{8\sin x}{(1-K)K\cos^2 x}\left[\frac{E_1\cos(x)+F_1\sin(x)}{E_1(2x+\sin 2x)-F_1\cos 2x}\right]+\Upsilon. \tag{21}$$

Case Id: $2-K+\Delta_0 K=0$

$$Y(x) = A(\cos x + x\sin x) + B\sin x, \tag{22}$$

$$\frac{\kappa p_r}{C} = \frac{2\sin x}{(1-K)K\cos^2 x}\left[\frac{G_1 x+H_1}{G_1(\cos x+x\sin x)+H_1\sin x}\right]+\frac{1}{K\cos^2 x}, \tag{23}$$

$$\frac{\kappa p_t}{C} = \frac{2\sin x}{(1-K)K\cos^2 x}\left[\frac{G_1 x+H_1}{G_1(\cos x+x\sin x)+H_1\sin x}\right]+\Upsilon, \tag{24}$$

where $\Upsilon = \frac{\Delta_0 K[(K-1)\sin^2 x - K]+(1-K)^2\cos^2 x}{(1-K)^2 K\cos^4 x}$.

B. Case II: $K > 1$, i.e., K is positive

Here, we extend our analysis by considering the positive values of K, and to solve Eq. (9) we adopt a similar approach to differentiate Eq. (9) with respect to Z. For this purpose we use another substitution, where $Z = \cosh x$ (hyperboloidal case) and $\frac{dY}{dZ} = \psi$; Eq. (9) takes the form

$$\frac{d^2\psi}{dx^2} - (2-K+\Delta_0 K)\psi = 0, \tag{25}$$

where $\frac{d\psi}{dx} = \sinh x \frac{d^2Y}{dZ^2}$, and $\frac{d^2\psi}{dx^2} = -\sinh^2 x \frac{d^3Y}{dZ^3} + \cosh x \frac{d^2Y}{dZ^2}$, respectively. To solve the second order homogeneous differential equation (25) we consider the following cases:

$$\text{Case IIa: } \psi = A_2\cos(nx) + B_2\sin(nx) \quad \text{if } 2-K+\Delta_0 K = -n^2, \tag{26a}$$

$$\text{Case IIb: } \psi = C_2\cosh(nx) + D_2\sinh(nx), \quad \text{if } 2-K+\Delta_0 K = n^2 (\neq 1), \tag{26b}$$

$$\text{Case IIc: } \psi = E_2\cosh(x) + F_2\sinh(x), \quad \text{if } 2-K+\Delta_0 K = 1, \tag{26c}$$

$$\text{Case IId: } \psi = G_2 x + H_2 \quad \text{if } 2-K+\Delta_0 K = 0, \tag{26d}$$

where A_2, B_2, C_2, D_2, E_2, F_2, G_2, and H_1 are arbitrary constants of integration, with $x = \cosh^{-1} Z = \cosh^{-1}\sqrt{\frac{K+Cr^2}{K-1}}$. Recalling Eq. (7) and plugged into the relevant equation we obtain the expression of energy density ($K > 1$) as

$$\frac{\kappa\rho}{C} = \frac{(3-K+K\cosh^2 x - \cosh^2 x)}{K(K-1)\sinh^4 x}. \tag{27}$$

Now proceeding the same as for $K < 0$, we consider the following cases for $K > 1$, and pressure components can be developed as follows:

Case IIa: $2-K+\Delta_0 K = -n^2$

$$Y(x) = \frac{1}{(n^2+1)}[\cosh x[A\cos(nx)+B\sin(nx)] + n\sinh x[A\sin(nx) - B\cos(nx)]], \tag{28}$$

$$\frac{\kappa p_r}{C} = \frac{2(n^2+1)}{(K-1)K\sinh^2 x}\left[\frac{A_2\cos(nx)+B_2\sin(nx)}{[A_2\cos(nx)+B_2\sin(nx)] + n\tanh x[A_2\sin(nx) - B_2\cos(nx)]}\right] - \frac{1}{K\sinh^2 x}, \tag{29}$$

$$\frac{\kappa p_t}{C}=\frac{2(n^2+1)}{(K-1)K\sinh^2 x}\left[\frac{A_2\cos(nx)+B_2\sin(nx)}{[A_2\cos(nx)+B_2\sin(nx)]+n\tanh x[A_2\sin(nx)-B_2\cos(nx)]}\right]+\Upsilon_1. \tag{30}$$

Case IIb: $2-K+\Delta_0 K=n^2(\neq 1)$

$$Y(x)=\frac{1}{(1-n^2)}[\cosh x[C_2\cosh(nx)+D_2\sinh(nx)]-n\sinh x[C_2\sinh(nx)-D_2\cosh(nx)]], \tag{31}$$

$$\frac{\kappa p_r}{C}=\frac{2(1-n^2)}{(K-1)K\sinh^2 x}\left[\frac{C_2\cosh(nx)+D_2\sinh(nx)}{[C_2\cosh(nx)+D_2\sinh(nx)]-n\tanh x[C_2\sinh(nx)-D_2\cosh(nx)]}\right]-\frac{1}{K\sinh^2 x}, \tag{32}$$

$$\frac{\kappa p_t}{C}=\frac{2(1-n^2)}{(K-1)K\sinh^2 x}\left[\frac{C_2\cosh(nx)+D_2\sinh(nx)}{[C_2\cosh(nx)+D_2\sinh(nx)]-n\tanh x[C_2\sinh(nx)-D_2\cosh(nx)]}\right]+\Upsilon_1. \tag{33}$$

Case IIc: $2-K+\Delta_0 K=1$

$$Y(x)=\frac{1}{4}[A\cosh 2x+B\sinh(2x)-2Bx], \tag{34}$$

$$\frac{\kappa p_r}{C}=\frac{8\cosh x}{(K-1)K\sinh^2 x}\left[\frac{E_2\cosh(x)+F_2\sinh(x)}{E_2\cosh 2x+F_2\sinh(2x)-2F_2 x}\right]-\frac{1}{K\sinh^2 x}, \tag{35}$$

$$\frac{\kappa p_t}{C}=\frac{8\cosh x}{(K-1)K\sinh^2 x}\left[\frac{E_2\cosh(x)+F_2\sinh(x)}{E_2\cosh 2x+F_2\sinh(2x)-2F_2 x}\right]+\Upsilon_1. \tag{36}$$

Case IId: $2-K+\Delta_0 K=0$

$$Y(x)=G_2(x\cosh x-\sinh x)+H_2\cosh x, \tag{37}$$

$$\frac{\kappa p_r}{C}=\frac{2\cosh x}{(K-1)K\sinh^2 x}\left[\frac{G_2 x+H_2}{G_2(x\cosh x-\sinh x)+H_2\cosh x}\right]-\frac{1}{K\sinh^2 x}, \tag{38}$$

$$\frac{\kappa p_t}{C}=\frac{2\cosh x}{(K-1)K\sinh^2 x}\left[\frac{G_2 x+H_2}{G_2(x\cosh x-\sinh x)+H_2\cosh x}\right]+\Upsilon_1, \tag{39}$$

where $\Upsilon_1=\frac{\Delta_0 K[(K-1)\cosh^2 x-K]-(1-K)^2\sinh^2 x}{(1-K)^2 K\sinh^4 x}$, and we have four sets of solutions corresponding to the positive and negative values of K. Following the standard procedure for stellar modeling one usually imposes some restrictions. In a realistic scenario, one can expect that the following conditions are satisfied throughout the stellar interior:

(i) the interior solution goes up to a certain radius R, where the spacetime is assumed not to possess an event horizon,
(ii) positive definiteness of the energy density and pressure at the center,
(iii) the density should be maximum at center and decreasing monotonically within $0<r<R$, i.e., the density gradient $d\rho/dr$ is negative within $0<r<R$,
(iv) the pressure should be maximum at center and decreasing monotonically within $0<r<R$, i.e., the pressure gradient dp/dr is also negative within $0<r<R$,
(v) the ratio of pressure and density should be less than unity within $0<r<R$, i.e., p/ρ should lie between 0 to 1 within the stellar model.

These features, positive density, positive pressure, and the absence of horizons, are the most important features characterizing a star. The task is now to check the well-behaved geometry and capability of describing realistic stars; we plot this in Fig. 1 (due to complexity of expression). For our stellar model, depending on the different values of K, the behavior of ρ, p_r, and p_t has been studied. Such analytical representations have been performed by using recent measurements of mass and radius of neutron stars, LMC X-4, SMC X-1, EXO 1785-248, SAX J1808.4-3658 (SS2), Her X-1, 4U 1538-52, PSR $1937+21$, Cen X-3, and SAX J1808.4-3658. Detailed expressions and value of constants that have been used in this work are given in Fig. 1, and will not be repeated here. It is evident from these plots that the energy density is maximum as $r\to 0$ and decreases towards the boundary.

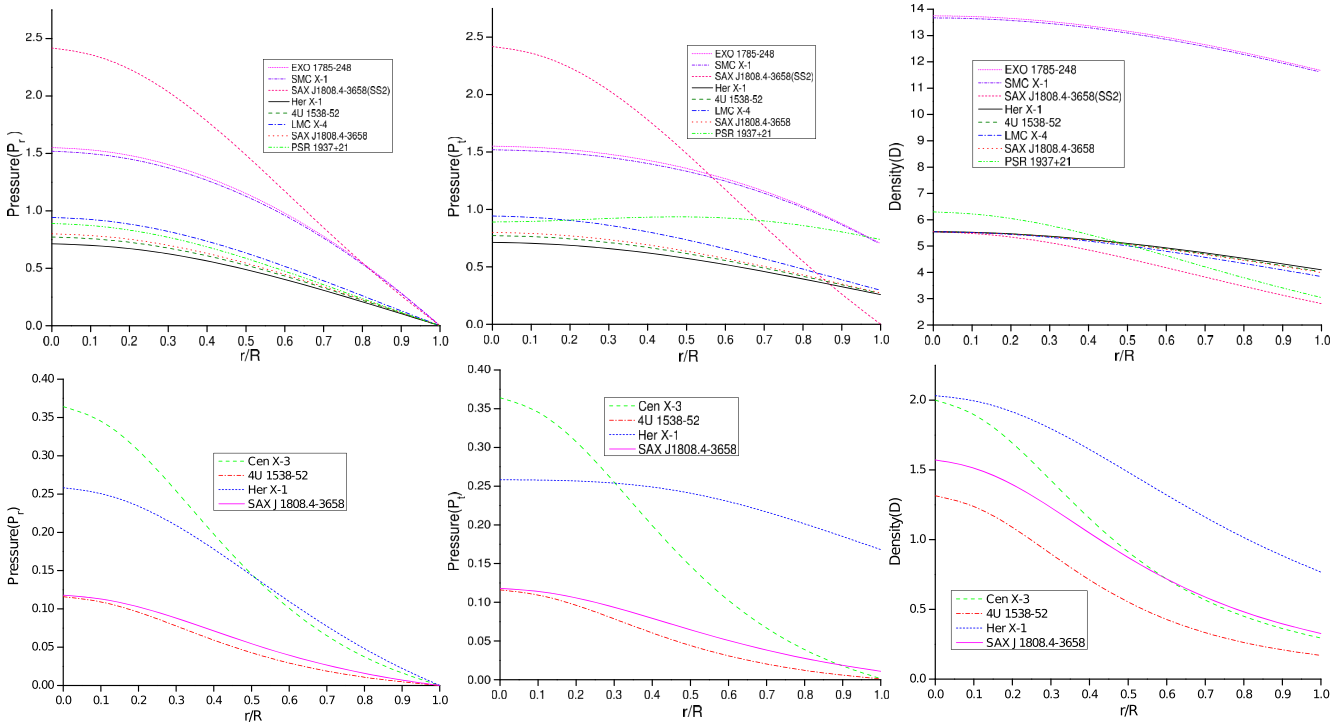

FIG. 1. From top left to right we have plotted the effective radial pressure ($P_r = \kappa p_r/C$), effective transverse pressure ($P_t = \kappa p_t/C$), and effective energy density ($D = \kappa\rho/C$) verses the radial coordinate (r/R) for Case I, in their normalized forms inside the star. In the lower graphs we repeat the same situation for Case II, where P_r, P_t, and D are dimensionless. The radial pressure (p_r), tangential pressure (p_t), and density (ρ) can be determined in the *CGS* unit as: $p_r = P_r \times C \times 4.81 \times 10^{47}$ dyne, $p_t = P_t \times C \times 4.81 \times 10^{47}$ dyne, $\rho = D \times C \times 5.35 \times 10^{26}$ gm/cm. The values of the parameter which we have used for graphical presentation are: (i) $K = -0.27898$, $C = 1.33 \times 10^{-13}$ cm^{-2}, $n = 0.1$ for EXO 1785-248 (Ia); (ii) K $= -0.28103$, $C = 1.52 \times 10^{-13}$ cm^{-2}, $n = 0.1$ for SMC X-1 (Ia); (iii) K $= -1.18$, $C = 1.37 \times 10^{-12}$ cm^{-2}, $n = 1.783$ for SAX J1808.4-3658 (SS2) (Ib); (iv) K $= -1.18$, $C = 3.07 \times 10^{-13}$ cm^{-2} for Her X-1 (Ic); (v) K $= -1.18$, $C = 3.47 \times 10^{-13}$ cm^{-2} for 4U 1538-52 (Ic); (vi) K $= -1.18$, $C = 3.21 \times 10^{-13}$ cm^{-2} for LMC X-4 (Ic); (vii) K $= -1.18$, $C = 3.49 \times 10^{-13}$ cm^{-2} for SAX J1808.4-3658 (Ic); (viii) K $= -0.91$, $C = 8.82 \times 10^{-13}$ cm^{-2} for PSR $1937 + 21$ (Id); (ix) K $= 3$, $C = 3.03 \times 10^{-12}$ cm^{-2}, $n = 0.99$ for Cen X-3 (IIa); (x) K $= 1.78$, $C = 4.71 \times 10^{-12}$ cm^{-2}, $n = 0.4796$ for 4U 1538-52 (IIb); (xi) K $= 3.1$, $C = 1.28 \times 10^{-12}$ cm^{-2} for Her X-1 (IIc); (xii) K $= 2.1$, $C = 2.78 \times 10^{-12}$ cm^{-2} for SAX J1808.4-3658 (IId). See Table I for more details.

Finally, we move on to describe the results obtained from our calculations, which are illustrated in Fig. 2; that anisotropy is zero at center and positive in the stellar interior, which implies that the tangential pressure (p_t) is always greater than the radial pressure (p_r). Finally, using the anisotropic fluid will simplify the comparison with isotropic solutions and is most often used for studying massive compact objects [79].

In addition to this central density, the central and surface pressures of compact stars are presented in Table II. It is intriguing to note that the maximum density at the center $\sim 10^{15}$ gm/cm^3, which is constrained with the argument by Ruderman [9] for anisotropic stellar configurations that can describe realistic neutron stars. For example, the millisecond pulsar SAX J1808.4-3658 (SS2) [74] with 1.3237 $M_\odot$ has the central density 4.06×10^{15} gm/cm^3 (the other results are given in Table II). Moreover, inside the star, p_r and $p_t > 0$, and the pressure decreases monotonically as we move away from the center, as is evident in Fig. (1). Furthermore, it has been shown that upper bound on the total compactness of a static spherically symmetric fluid in the form of $2M/R \leq 8/9$ [54]. As one can see, we have explicitly derived Buchdahl's inequality for an anisotropic fluid star, which matches exactly with the limit derived for the uniform density star (see Table II).

IV. EXTERIOR SOLUTIONS

To proceed further, the interior spacetime metric (1) should be matched with the Schwarzschild exterior solution at the boundary of the star ($r = R$). In principle the radius R is a natural parameter, where the radial pressure vanishes, i.e., $p_r(R) = 0$. The exterior vacuum solution is then given by the Schwarzschild metric

$$ds^2 = -\left(1 - \frac{2M}{r}\right)dt^2 + \left(1 - \frac{2M}{r}\right)^{-1}dr^2 + r^2(d\theta^2 + \sin^2\theta d\phi^2), \tag{40}$$

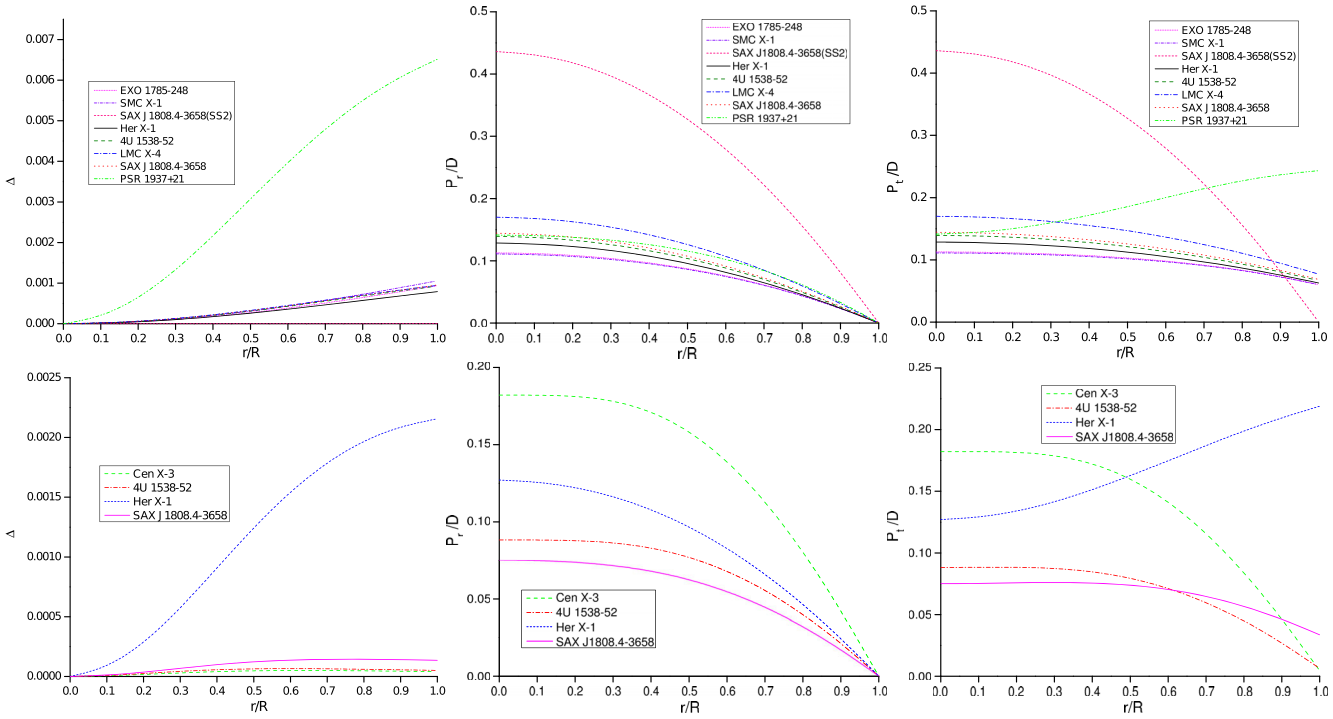

FIG. 2. Variation of anisotropy factor Δ (in km^{-2}) for effective pressure-density ratio P_i/D vs. radial coordinate r/R for Case I (upper panel) and Case II (lower panel). For plotting these graphs, we have employed the same dataset as used in Fig. 1.

where M is the total mass of the gravitational system, and it is given by

$$M_{\rm tot}(r) = \int_0^r 4\pi r^2 \rho dr. \tag{41}$$

At this stage the interior solution must be matched to the vacuum exterior Schwarzschild metric. We match two spacetimes across the boundary surface using the Darmois-Israel formalism [83], which are tantamount to the following two conditions across the boundary surface $r = R$:

$$e^{-\lambda} = 1 - \frac{2M}{R}, \quad \text{and} \quad e^{\nu} = y^2 = 1 - \frac{2M}{R}, \tag{42}$$

$$p_r(r = R) = 0. \tag{43}$$

Now, using the conditions (42) and (43), we can fix the values of arbitrary constants. Thus, the boundary condition provides a full set of expressions for arbitrary constants A_1 to H_1 (when $K < 0$) and A_2 to H_2 (when $K > 1$) as follows:

Case Ia: $\frac{A_1}{B_1} = \frac{n(1-K)\cosh(nx_1)\csc(x_1)+(3-K+2n^2)\sec(x_1)\sinh(nx_1)}{(-3+K-2n^2)\cosh(nx_1)\sec x_1+n(K-1)\csc x_1\sinh(nx_1)}$,

Case Ib: $\frac{C_1}{D_1} = \frac{n(K-1)\cos(nx_1)\csc x_1+(-3+K+2n^2)\sec x_1\sin(nx_1)}{(3-K-2n^2)\cos(nx_1)\sec x_1+(K-1)n\csc x_1\sin(nx_1)}$,

Case Ic: $\frac{E_1}{F_1} = \frac{(1-K)\cos(2x_1)-8\sin^2 x_1}{4\sin 2x_1-(K-1)[2x_1+\sin(2x_1)]}$,

Case Id: $\frac{G_1}{H_1} = \frac{2\sin x_1+(1-K)\sin x_1}{(K-1)\cos x_1+x_1[-2\sin x_1+(K-1)\sin x_1]}$,

Case IIa: $\frac{A_2}{B_2} = \frac{n(K-1)\cos(nx_2)\mathrm{sech}(x_2)+(3-K+2n^2)\mathrm{csch}(x_2)\sin(nx_2)}{(-3+K-2n^2)\cos(nx_2)\mathrm{csch}(x_2)+n(K-1)\mathrm{sech}(x_2)\sin(nx_2)}$,

Case IIb: $\frac{C_2}{D_2} = \frac{n(K-1)\cosh(nx_2)\mathrm{sech}(x_2)+(-3+K+2n^2)\mathrm{csch}(x_2)\sinh(nx_2)}{(3-K-2n^2)\cosh(nx_2)\mathrm{csch}(x_2)+n(K-1)\mathrm{sech}(x_2)\sinh(nx_2)}$,

Case IIc: $\frac{E_2}{F_2} = \frac{-8\sinh x_2\cosh x_2+(K-1)[-2x_2+\sinh(2x_2)]}{8\cosh^2 x_2-(K-1)\cosh(2x_2)}$,

Case IId: $\frac{G_2}{H_2} = \frac{2\cosh x_2+(1-K)\cosh x_2}{-2x_2\cosh x_2+(K-1)x_2\cosh x_2+\sinh x_2-K\sinh x_2}$,

where $x_1 = \sin^{-1}\sqrt{\frac{K+CR^2}{K-1}}$ and $x_2 = \cosh^{-1}\sqrt{\frac{K+CR^2}{K-1}}$.

Here, we want to investigate the gravitational mass and radius of neutron stars. With the condition $e^{-\lambda} = 1 - \frac{2M}{R}$, it is useful to write the total mass in the following form:

$$M = \frac{(K-1)CR^3}{2K(1+CR^2)}. \tag{44}$$

We now present our results for the static neutron star models, showing the total mass M (in solar masses $M_\odot$) versus the physical radius R (in km) in Fig. 3. In this figure, all values are considered in the same succession as mentioned in Fig. 1.

We shall now use the general relativistic effect of gravitational redshift by the relation $z_S = \Delta\lambda/\lambda_e = \frac{\lambda_0-\lambda_e}{\lambda_e}$, where λ_e is the emitted wavelength at the surface of a nonrotating star, and λ_0 is the observed wavelength received at radial coordinate r. In the weak-field limit, gravitational redshift from the surface of the star as measured by a distant observer $(g_{tt} \to -1)$ is given by

$$1 + z_S = |g_{tt}(R)|^{-1/2} = \left(1 - \frac{2M}{R}\right)^{-1/2}, \tag{45}$$

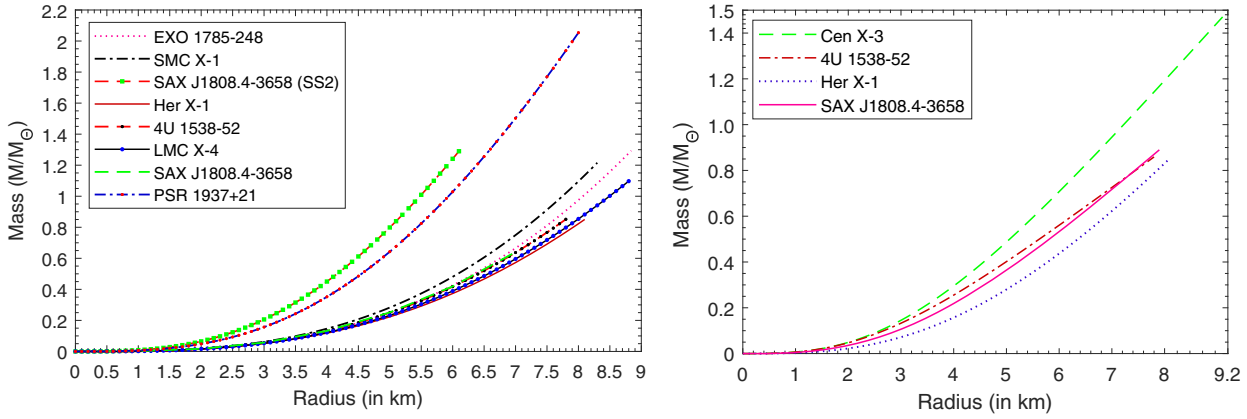

FIG. 3. Variation of the total mass normalized in units of Solar mass ($M/M_\odot$) with the total radius R for Case I (left panel) and Case II (right panel), respectively.

where $g_{tt}(R) = e^{\nu(R)} = (1 - \frac{2M}{R})$ is the metric function. It was shown earlier by Buchdahl [54] that for spherically symmetric distribution of a prefect fluid the gravitational redshift is $z_s < 2$. However, different arguments have been put forward for the existence of anisotropy star models which turn out to be 3.84, as suggested by [84,85]. On the other hand, in studying general restrictions for the redshift for anisotropic stars, Bohmer and Harko [86] showed that this value could be increased up to $z_s \leq 5$, which is consistent with the bound $z_s \leq 5.211$ obtained by Ivanov [34]. We perform the whole calculations for redshift of the enlisted compact objects by taking the same values, which we have used for graphical presentation in Fig. 4. We are mostly interested in bounds on surface redshift for spherically symmetric stellar structures, and our results are quite satisfactory.

V. PHYSICAL FEATURES OF ANISOTROPIC MODELS

We now study physical properties of the stellar configuration made up of anisotropic fluids by performing some analytical calculations. We analyzed the stability problem by considering the modified Tolman-Oppenheimer-Volkoff (TOV) equation and checking the causality conditions within the fluid. With these one can determinate the value of the speed of sound across a given star. Finally, we investigate the types of compact objects that might arise from these solutions and how to restrict the model arbitrariness.

A. Causality condition

In addition to the positivity of density and pressure profiles, we shall pay special and particular attention to the condition of bounding sound speeds (radial and tangential directions) within the matter distribution. Essentially, we fix $c = 1$ and investigate the sound speed for anisotropic fluid distribution. It is obvious that the velocity of sound is less than the velocity of light, i.e., $0 < v_r^2 = dp_r/d\rho < 1$ and $0 < v_r^2 = dp_t/d\rho < 1$. The stability of the fluid sphere with internal pressure anisotropy was also probed by Herrera [87] and his collaborators. Here, we consider Case I and Case II separately, and the expression for velocity of sound is as follows:

Case Ia:

$$\frac{dp_r}{d\rho} = \frac{N_1}{S_1}, \tag{46}$$

$$\frac{dp_t}{d\rho} = \frac{N_1}{S_1} + \frac{\Delta_0[2\cos^2 x \sin x(K-1) + 4\sin x((K-1)\sin^2 x - K)]}{(K-1)^2\cos^5 x}, \tag{47}$$

Case Ib:

$$\frac{dp_r}{d\rho} = \frac{N_2}{S_1}, \tag{48}$$

$$\frac{dp_t}{d\rho}=\frac{N_2}{S_1}+\frac{\Delta_0[2\cos^2 x\sin x(K-1)+4\sin x((K-1)\sin^2 x-K)]}{(K-1)^2\cos^5 x}, \tag{49}$$

Case Ic:

$$\frac{dp_r}{d\rho}=\frac{N_3}{S_1}, \tag{50}$$

$$\frac{dp_t}{d\rho}=\frac{N_3}{S_1}+\frac{\Delta_0[2\cos^2 x\sin x(K-1)+4\sin x((K-1)\sin^2 x-K)]}{(K-1)^2\cos^5 x}, \tag{51}$$

Case Id:

$$\frac{dp_r}{d\rho}=\frac{N_4}{S_1}, \tag{52}$$

$$\frac{dp_t}{d\rho}=\frac{N_4}{S_1}+\frac{\Delta_0[2\cos^2 x\sin x(K-1)+4\sin x((K-1)\sin^2 x-K)]}{(K-1)^2\cos^5 x}, \tag{53}$$

Case IIa:

$$\frac{dp_r}{d\rho}=\frac{N_5}{S_2}, \tag{54}$$

$$\frac{dp_t}{d\rho}=\frac{N_5}{S_5}+\frac{\Delta_0[2\cosh x\sinh^2 x(K-1)-4\cosh x((K-1)\cosh^2 x-K)]}{(K-1)^2\sinh^5 x}, \tag{55}$$

Case IIb:

$$\frac{dp_r}{d\rho}=\frac{N_6}{S_2}, \tag{56}$$

$$\frac{dp_t}{d\rho}=\frac{N_6}{S_2}+\frac{\Delta_0[2\cosh x\sinh^2 x(K-1)-4\cosh x((K-1)\cosh^2 x-K)]}{(K-1)^2\sinh^5 x}, \tag{57}$$

Case IIc:

$$\frac{dp_r}{d\rho}=\frac{N_7}{S_2}, \tag{58}$$

$$\frac{dp_t}{d\rho}=\frac{N_7}{S_2}+\frac{\Delta_0[2\cosh x\sinh^2 x(K-1)-4\cosh x((K-1)\cosh^2 x-K)]}{(K-1)^2\sinh^5 x}, \tag{59}$$

Case IId:

$$\frac{dp_r}{d\rho}=\frac{N_8}{S_2}, \tag{60}$$

$$\frac{dp_t}{d\rho}=\frac{N_8}{S_2}+\frac{\Delta_0[2\cosh x\sinh^2 x(K-1)-4\cosh x((K-1)\cosh^2 x-K)]}{(K-1)^2\sinh^5 x}, \tag{61}$$

where the expressions of used coefficients N_1, N_2, N_3, N_4, N_5, N_6, N_7, N_8, S_1, and S_2 in Eqs. (46)–(61) are given in Appendix B.

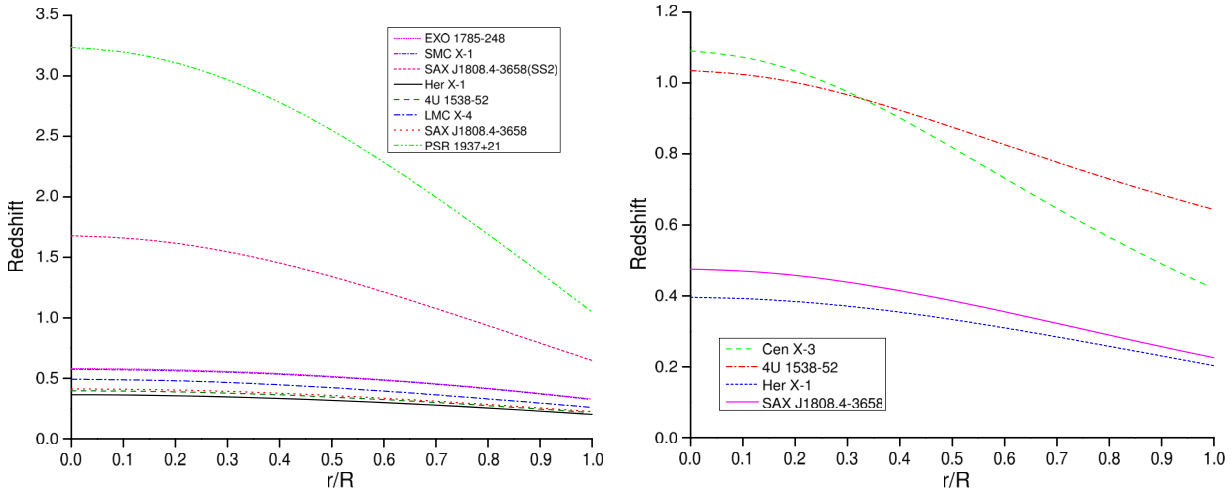

FIG. 4. Behavior of redshift (left figure for Case I and right figure for Case II) vs. radial coordinate r/R which have been plotted for different compact star candidates. For the purpose of plotting this graph, we have employed the dataset of values as same as Fig. 1.

In this analytical approach, we use the graphical representation to represent the velocity of sound due to the complexity of the expression. Considering all expressions for both Cases I and II, we have plotted Fig. 5. In Fig. 5 we plot for radial and transverse velocity of sound when $K < 0$ (top figures), and $K > 1$ (bottom figures) for compact star candidates LMC X-4, SMC X-1, EXO 1785-248, SAX J1808.4-3658 (SS2), Her X-1, 4U 1538-52, PSR $1937 + 21$, Cen X-3, and SAX J1808.4-3658. Our investigation shows that our equation of state for anisotropic matter satisfies the causality condition. From Fig. 5, it is interesting to note that the velocity of sound is decreasing for the stars SAX J1808.4-3658 (SS2) (Case Ib), LMC X-4 (Case Ic), 4U 1538-52 (Case Ic), Her X-1 (Case Ic), SAX J1808.4-3658 (Case Ic), Her X-1 (Case IIc), and increasing for SMC X-1 (Case Ia), EXO 1785-248 X-1 (Case Ia), PSR $1937 + 21$ (Case Id), Cen X-3 (Case IIa), 4U 1538-52 (Case IIb), SAX J1808.4-3658 (Case IId) towards the boundary which implies that our solution is well behaved for the above cases. The decreasing features of the velocities are appearing in the present compact star model due to the presence of anisotropy only because the velocity of sound is not decreasing for the Buchdahl metric in charged as well as uncharged perfect fluid solutions [81,82]. Now, we focus on investigation of the adiabatic index, energy conditions, and hydrostatic equilibrium for compact stars in accordance to their mass and radius ratio.

B. Adiabatic index

For a specific energy density, the rigidity of the EoS can be described by the adiabatic index. On the other hand, the adiabatic index also characterizes the stability of relativistic as well as nonrelativistic compact star models. Following the work of Chandrasekhar [88], many authors [89–92] have discussed the dynamical stability of the stellar system against an infinitesimal adiabatic perturbation corresponding to radial pressure. For any dynamically stable stellar system, Heintzmann and Hillebrandt [11] have suggested that the radial adiabatic index must be more than $\frac{4}{3}$ at all interior points of the compact star. The radial adiabatic index γ_r in our system is given as

$$\gamma_r = \frac{p_r + \rho}{p_r}\frac{dp_r}{d\rho} = \frac{p_r + \rho}{p_r} v_r^2. \tag{62}$$

The graphical representation of the radial adiabatic index is given by Fig. 6. For this figure it is clear that the value of the adiabatic index corresponding to radial pressure is more than $\frac{4}{3}$ at all interior points for each different compact star model.

C. Energy conditions

Here we analyze the energy conditions according to relativistic classical field theories of gravitation. In the context of GR the energy conditions are local inequalities that process a relation between matter density and pressure obeying certain restrictions. Many plausible physical constraints have been proposed, such as the positive mass theorem [93], the censorship theorem [94,95], the singularity theorems [96], and various constraints on black hole surface gravity [97], but perhaps the most important and far-reaching applications are the energy conditions. There are several different ways to formulate the energy conditions, but we will focus here only on (i) the null energy condition (NEC), (ii) the weak energy condition (WEC), and (iii) the strong energy condition (SEC). In summary:

$$\textbf{NEC}: \ \rho(r) + p_r \geq 0, \tag{63a}$$

$$\textbf{WECr}: \ \rho + p_r \geq 0, \quad \text{and} \quad \rho(r) \geq 0, \tag{63b}$$

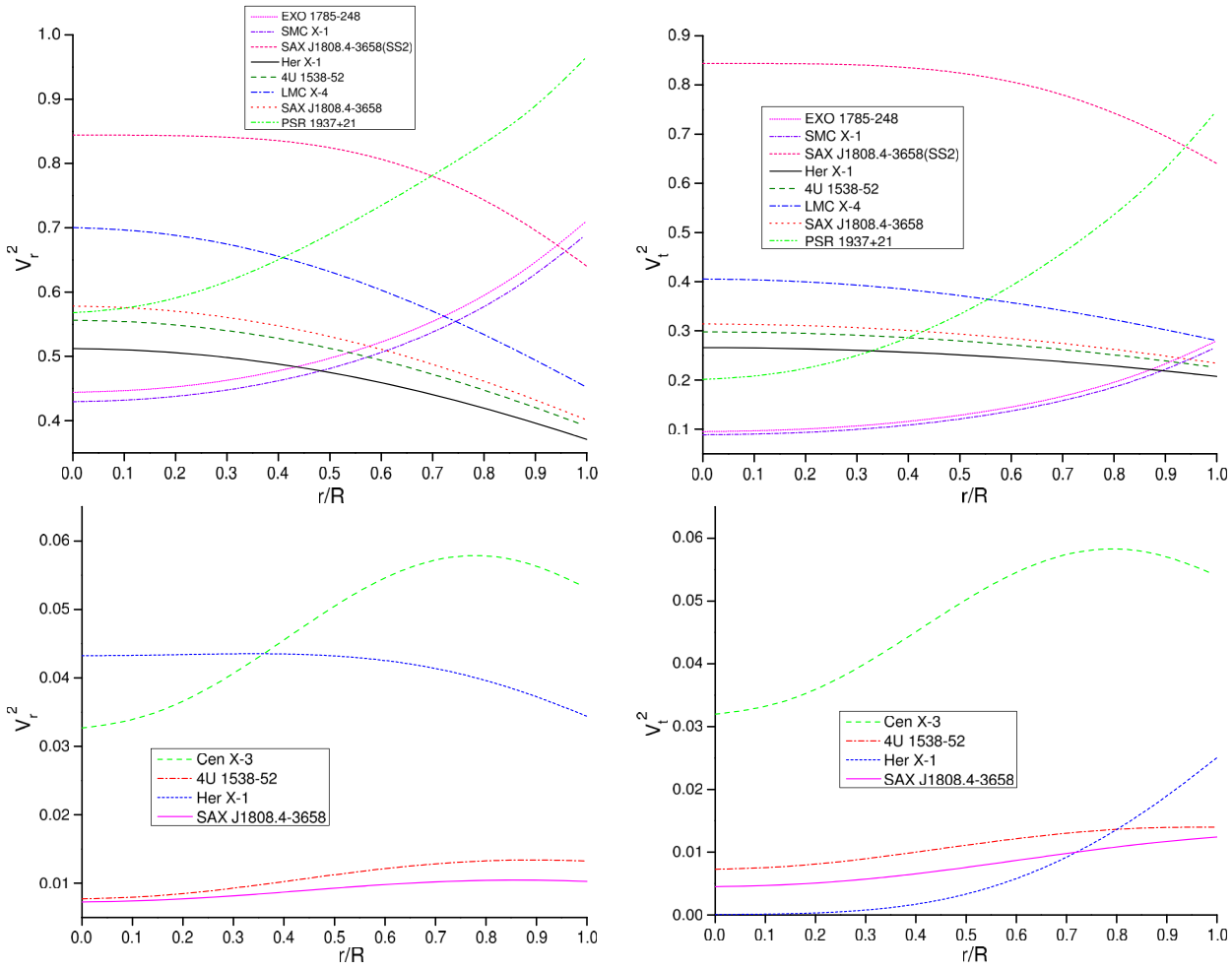

FIG. 5. Variation of radial and transverse speeds of sound have been plotted for respective stellar models for Case I (top figures) and Case II (bottom figures). We use the same data as in Fig. 1.

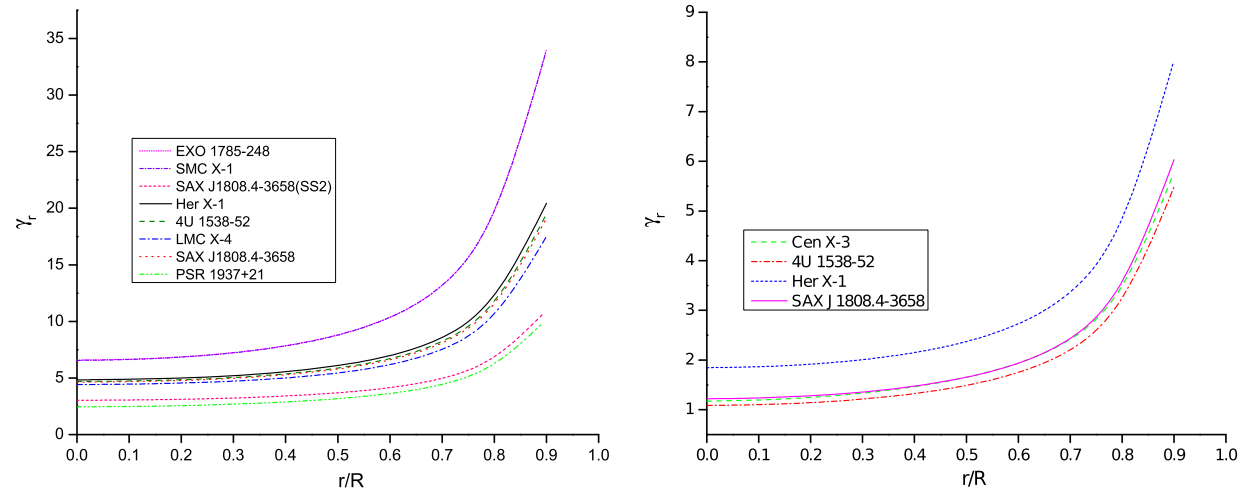

FIG. 6. Adiabatic index (γ_r) (left figure for Case I and right for Case II) vs. radial coordinate r/R which have been plotted for different compact star candidates. For the purpose of plotting this graph, we have employed the dataset of values as same as in Fig. 1.

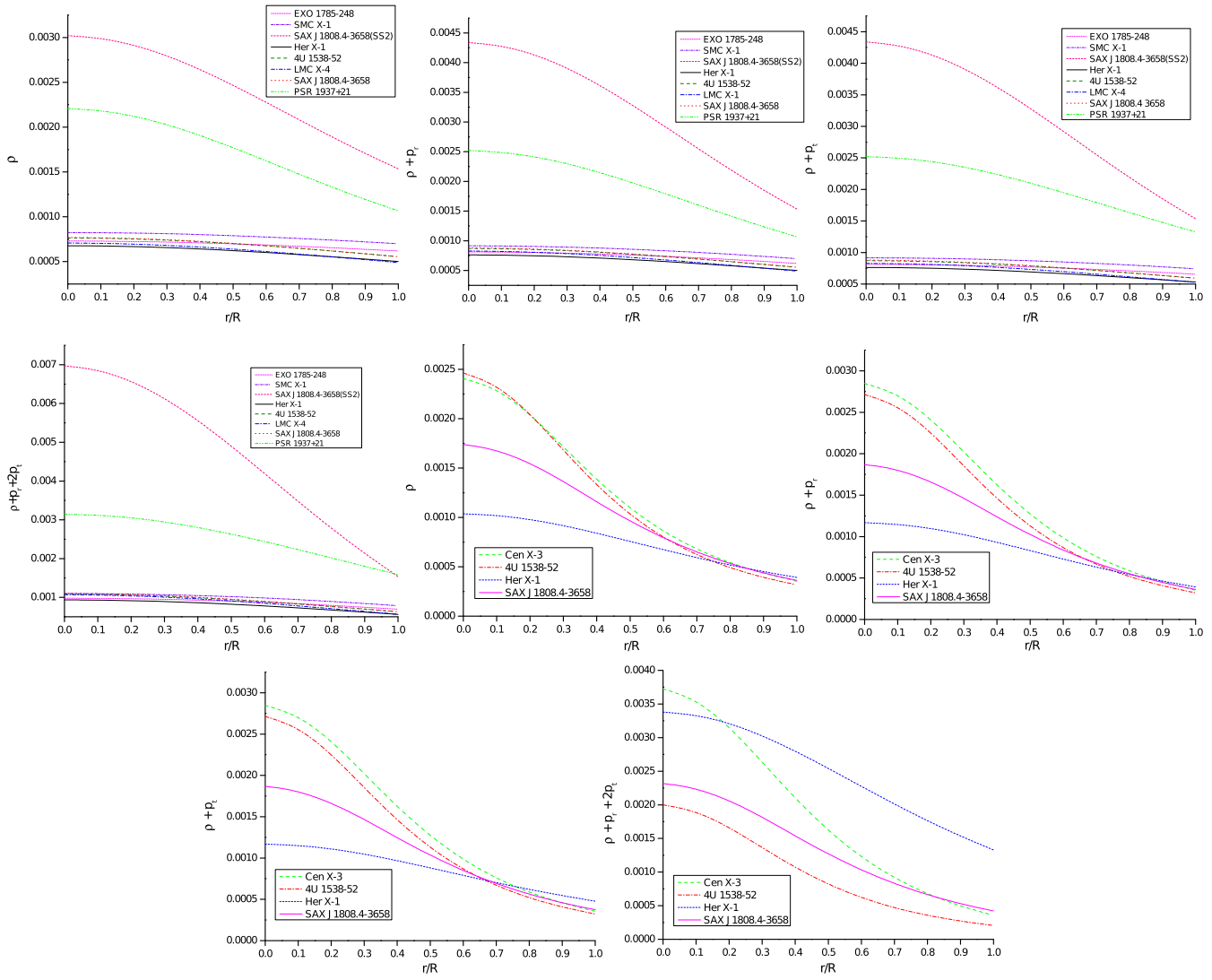

FIG. 7. The different energy conditions (in km^{-2}) diagrammed in the model for Case I and Case II have been plotted with respect to radial coordinate r/R, where the first four graphs describe energy conditions corresponding to Case I while the next four graphs correspond to Case II.

$$\textbf{WECt}: \rho + p_t \geq 0, \quad \text{and} \quad \rho(r) \geq 0, \tag{63c}$$

$$\textbf{SEC}: \rho + p_r + 2p_t \geq 0. \tag{63d}$$

We derive precisely all the forms of energy conditions for both cases by plugging the values of energy density and respective pressure equations. The resulting graph in Fig. 7 shows that all the inequalities hold simultaneously for the sources considered here.

D. Generalized TOV equation

The Tolman-Oppenheimer-Volkoff (TOV) equation is used to constrain the structure of a spherically symmetric body (both isotropic and anisotropic fluid models) that is covered regarding stars in hydrostatic equilibrium. Here, we start by explaining the different forces, namely, gravitational, hydrostatic, and anisotropic forces, respectively. The governing generalized TOV equation for anisotropic fluid distribution is given by [98,99]

$$-\frac{M_G(\rho + p_r)}{r^2} e^{\frac{\lambda-\nu}{2}} - \frac{dp}{dr} + \frac{2(p_t - p_r)}{r} = 0, \tag{64}$$

where M_G is the effective gravitational mass inside the fluid sphere of radius "r", and defined by

$$M_G(r) = \frac{1}{2} r^2 \nu' e^{(\nu-\lambda)/2}. \tag{65}$$

Now, plugging the value of $M_G(r)$ in Eq. (64), we get

$$-\frac{\nu'}{2}(\rho + p_r) - \frac{dp_r}{dr} + \frac{2(p_t - p_r)}{r} = 0. \tag{66}$$

The above TOV equation describes the equilibrium condition for anisotropic fluid spheres subject to gravitational, hydrostatic, and anisotropic forces due to the anisotropic pressure. Combining all forces we have the following form:

$$F_g + F_h + F_a = 0. \tag{67}$$

Now, we start by explaining Eq. (67) from an equilibrium point of view, where three different components are gravitational (F_g), hydrostatic (F_h), and anisotropic (F_a) forces, respectively, with the following expression:

$$F_g = -\frac{\nu'}{2}(\rho + p_r), F_h = -\frac{dp_r}{dr}, \quad \text{and}$$
$$F_a = \frac{2(p_t - p_r)}{r} = \frac{2\Delta}{C}. \tag{68}$$

Here, the anisotropy force (F_a) takes the following form for both Cases I and II, which turns out to be

$$\text{Case I: } F_a = \frac{\Delta_0[(K-1)\sin^2 x - K]}{(K-1)^2\cos^4 x} \quad \text{and} \quad \text{Case II: } F_a = \frac{\Delta_0[(K-1)\cosh^2 x - K]}{(K-1)^2\sinh^4 x}, \tag{69}$$

and the other components are written in an explicit form:

Case Ia:

$$F_h = N_1\left[\frac{Cr}{\sin x\cos x(K-1)}\right], \tag{70}$$

$$F_g = -\frac{Cr(1+n^2)}{\sin^2 x(K-1)}\left[\frac{A_1\cosh(nx) + B_1\sinh(nx)}{\cosh(nx)(A_1 + B_1 n\cot x) + \sinh(nx)(A_1 n\cot x + B_1)}\right](\rho + p_r), \tag{71}$$

Case Ib:

$$F_h = N_2\left[\frac{Cr}{\sin x\cos x(K-1)}\right], \tag{72}$$

$$F_g = -\frac{Cr(1-n^2)}{\sin^2 x(K-1)}\left[\frac{C_1\cos(nx) + D_1\sin(nx)}{C_1\cos(nx) + D_1\sin(nx) - n\cot x(C_1\sin(nx) - D_1\cos(nx))}\right](\rho + p_r), \tag{73}$$

Case Ic:

$$F_h = N_3\left[\frac{Cr}{\sin x\cos x(K-1)}\right], \tag{74}$$

$$F_g = -\frac{8Cr}{\sin x(K-1)}\left[\frac{E_1\cos(x) + F_1\sin(x)}{E_1(2x + \sin 2x) - F_1\cos 2x}\right](\rho + p_r), \tag{75}$$

Case Id:

$$F_h = N_4\left[\frac{Cr}{\sin x\cos x(K-1)}\right], \tag{76}$$

$$F_g = -\frac{Cr}{\sin x(K-1)}\left[\frac{G_1(x) + H_1}{G_1(\cos x + x\sin x) + H_1\sin x}\right](\rho + p_r), \tag{77}$$

Case IIa:

$$F_h = N_5\left[\frac{Cr}{\sinh x\cosh x(K-1)}\right], \tag{78}$$

$$F_g = -\frac{Cr(1+n^2)}{\cosh^2 x(K-1)}\left[\frac{A_2\cos(nx)+B_2\sin(nx)}{A_2\cos(nx)+B_2\sin(nx)+n\tanh x(A_2\sin(nx)-B_2\cos(nx))}\right](\rho+p_r), \tag{79}$$

Case IIb:

$$F_h = N_6\left[\frac{Cr}{\sinh x\cosh x(K-1)}\right], \tag{80}$$

$$F_g = -\frac{Cr(1-n^2)}{\cosh^2 x(K-1)}\left[\frac{C_2\cosh(nx)+D_2\sinh(nx)}{[C_2\cosh(nx)+D_2\sinh(nx)]-n\tanh x[C_2\sinh(nx)+D_2\cosh(nx)]}\right](\rho+p_r), \tag{81}$$

Case IIC:

$$F_h = N_7\left[\frac{Cr}{\sinh x\cosh x(K-1)}\right], \tag{82}$$

$$F_g = -\frac{8Cr}{\cosh x(K-1)}\left[\frac{E_2\cosh x+F_2\sinh x}{E_2\cosh 2x+F_2(\sinh 2x-2x)}\right](\rho+p_r), \tag{83}$$

Case IId:

$$F_h = N_8\left[\frac{Cr}{\sinh x\cosh x(K-1)}\right], \tag{84}$$

$$F_g = -\frac{Cr}{\cosh x(K-1)}\left[\frac{G_2(x)+H_2}{G_2(x\cosh x-\sinh x)+H_2\cosh x}\right](\rho+p_r). \tag{85}$$

In order to evaluate equilibrium conditions, the hydrostatic equilibrium diagrams obtained for the eight different compact stars are shown in Fig. 8. From a mathematical point of view, one can see from Fig. 8 that the gravitational force (F_g) is dominating over the hydrostatic (F_h) and anisotropic (F_a) forces, which is counter balanced by the joint action of hydrostatic (F_h) and anisotropic (F_a) forces. From Fig. 8, we see that the force components F_g, F_h, and F_a of the TOV equation are regular and finite at the origin as well as on the surface of the star. Moreover, we also observe some other interesting features of force components corresponding to each star which are as follows: The hydrostatic force (F_h) and gravitational force (F_g) are increasing monotonically throughout within the stellar models and attain their maximum values on the boundary corresponding to the stars (i) EXO 1785-248, (ii) SMC X-1, while for other stars, namely (iii) SAX J1808.4-3658 (SS2)-1, (iv) Her X-1, (v) 4U 1538-52, (vi) LMC X-4, (vii) SAX J1808.4-3658, (viii) PSR 1937 + 21 (for Case I), and (ix) Cen X-3, (x) 4U 1538-52, (xi) Her X-1, (xii) SAX J1808.4-3658 (for Case II), the forces F_h and F_g increase first and reach their maximum value at some point r/R within the stellar model, and thereafter start decreasing towards the respective boundary. On the other hand, the anisotropic force F_a is increasing monotonically towards the surface boundary corresponding to each obtained star. From Fig. 8, we also note that the anisotropic force F_a has much less of an effect compared to the hydrostatic force F_h and the gravitational force F_g for the stars, namely (iii) SAX J1808.4-3658(SS2) (for Case I), and (ix) Cen X-3, (x) 4U 1538-52 (for Case II).

E. The equation of state

Here we derive the relation between the most important features of neutron stars, which is an equation of state (EoS), i.e., a relation between pressure and density. The EoS of neutron star matter at the inner core, where most of the mass resides, is not well constrained. It is worthwhile to mention that different EoS lead to different mass-radius (M-R) relations. To explain the structural properties of compact star models at high densities, several authors have proposed that the EoS $P = P(\rho)$ should be well approximated by a linear function of the energy density ρ [100–102]. Some authors have also expressed more convincing approximated forms of the EoS $P = P(\rho)$ as a linear function of energy density ρ (for more details see [103–105]). In order to reach that aim, we start our calculation by writing the EoS in a linear function form, i.e., $P = P(\rho)$.

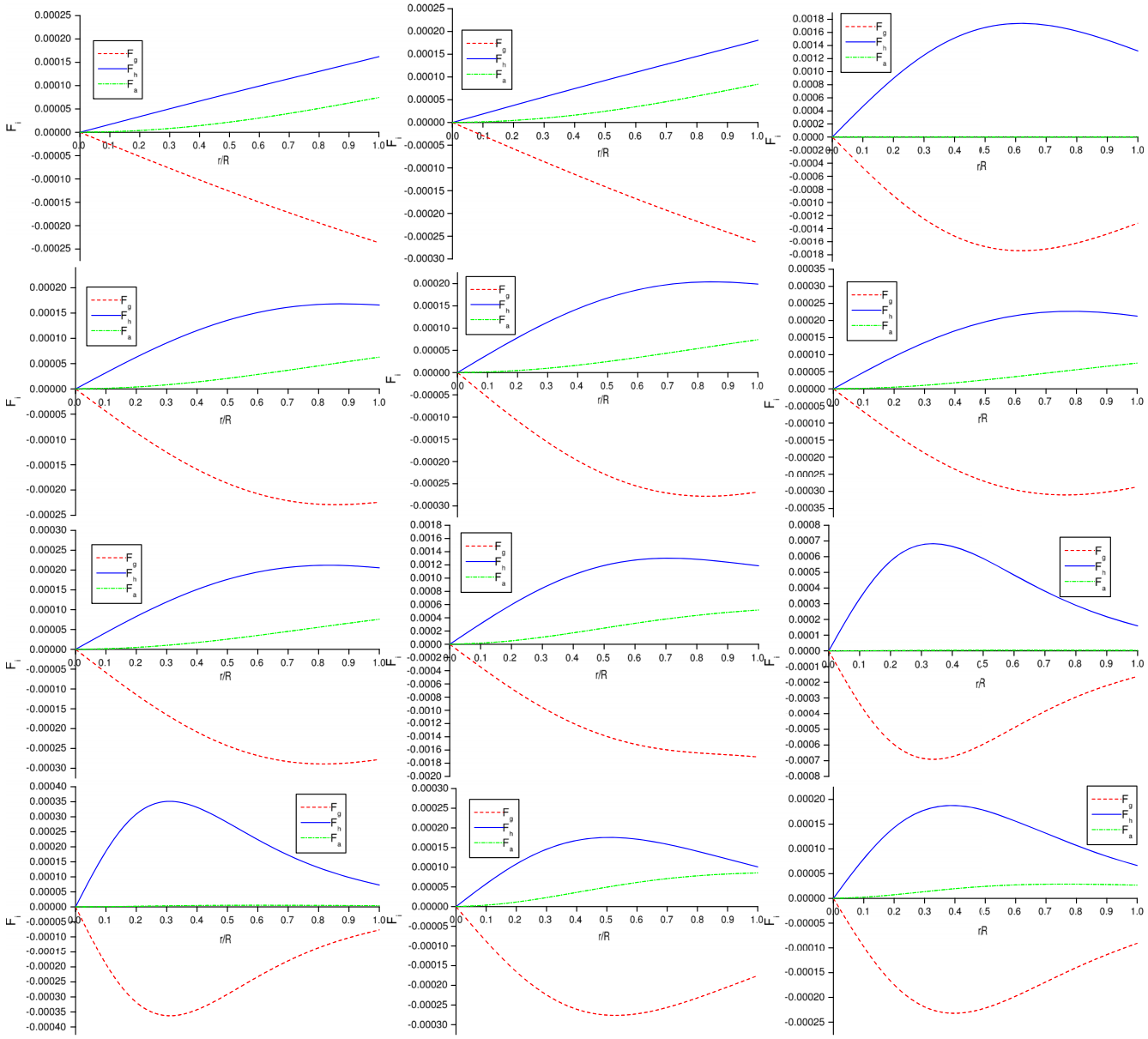

FIG. 8. Variation of different forces (in km^{-3} with $G = c = 1$) with respect to radial coordinate r/R. For plots we have drawn (i) EXO 1785-248, (ii) SMC X-1, and (iii) SAX J1808.4-3658(SS2)-1, from left to right in the first row. In the second row (iv) Her X-1, (v) 4U 1538-52, and (vi) LMC X-4, have been plotted. In the third and fourth rows (vii) SAX J1808.4-3658, (viii) PSR 1937 + 21, (ix) Cen X-3, (x) 4U 1538-52, (xi) Her X-1, and (xii) SAX J1808.4-3658 have been plotted for Cases I and II, respectively.

1. Case I: For $K < 0$, i.e., K is negative

$$p_r = \frac{C}{\kappa(1+\tilde{\rho}_1)K}\left[1 - K + \frac{2(1+n^2)[\sinh(n\tilde{\rho})f_1(\tilde{\rho}_s) + \cosh(n\tilde{\rho})f_2(\tilde{\rho}_s)]}{\cosh(n\tilde{\rho})(n\cosh(n\tilde{\rho}_s)(-f_3) + \sinh(n\tilde{\rho}_s)f_4) + \sinh(n\tilde{\rho})f_5}\right], \quad \text{Case Ia} \tag{86}$$

$$p_r = \frac{C}{\kappa(1+\tilde{\rho}_1)K}\left[1 - K + \frac{2(1-n^2)[-\sin(n\tilde{\rho})f_6(\tilde{\rho}_s) + \cos(n\tilde{\rho})f_7(\tilde{\rho}_s)]}{\cos(n\tilde{\rho})[n\cos(n\tilde{\rho}_s)f_8 - \sin(n\tilde{\rho}_s)f_9) + \sin(n\tilde{\rho}]f_{10}}\right], \quad \text{Case Ib} \tag{87}$$

$$p_r = \frac{C}{\kappa(1+\tilde{\rho}_1)K}\left[1 - K + \frac{8\sin(\tilde{\rho})[4\cos(\tilde{\rho}) + (K-5)\cos(\tilde{\rho} - 2\tilde{\rho}_s) + 2\tilde{\rho}_s(K-1)\sin(\tilde{\rho})]}{8\tilde{\rho} - 2\tilde{\rho}_s(K-1)\cos(2\tilde{\rho}) + (K-5)f_{11} + 4\sin(2\tilde{\rho})}\right], \quad \text{Case Ic} \tag{88}$$

$$p_r = \frac{C(3-K)[f_{12}+(1-K)\cos(\tilde{\rho})\sin(\tilde{\rho}_s)-f_{13}\sin(\tilde{\rho}_s)]}{\kappa(1+\tilde{\rho}_1)K[-f_{12}+((K-3)\cos(\tilde{\rho})+f_{13})\sin(\tilde{\rho_s})]}, \qquad \text{Case Id} \tag{89}$$

where, for notational convenience, we use

$\tilde{\rho} = \sin^{-1}\sqrt{\frac{K+\tilde{\rho}_1}{K-1}}$, $\tilde{\rho}_1 = \frac{(K-1-2\rho_1 K)\pm\sqrt{1-2K-8\rho_1 K+K^2+8\rho_1 K^2}}{2\rho_1 K}$, $\rho_1 = \frac{\kappa\rho}{C}$,

$\tilde{\rho}_s = \sin^{-1}\sqrt{\frac{K+\tilde{\rho}_{1s}}{K-1}}$, $\tilde{\rho}_{1s} = \frac{(K-1-2\rho_{1s} K)\pm\sqrt{1-2K-8\rho_1 K+K^2+8\rho_{1s} K^2}}{2\rho_{1s} K}$, $\rho_{1s} = \frac{\kappa\rho_s}{C}$,

$f_1(\tilde{\rho}_s) = (-2n^2+K-3)\cosh(n\tilde{\rho}_s)\sec(\tilde{\rho}_s)+n(K-1)\csc(\tilde{\rho}_s)\sinh(n\tilde{\rho}_s)$,

$f_2(\tilde{\rho}_s) = n(1-K)\cosh(n\tilde{\rho}_s)\csc(\tilde{\rho}_s)+(2n^2-K+3)\sec(\tilde{\rho}_s)\sinh(n\tilde{\rho}_s)$,

$f_3 = (K-1)\csc(\tilde{\rho}_s)+(2n^2-K+3)\cot(\tilde{\rho})\sec(\tilde{\rho}_s)$, $f_4 = n^2(K-1)\cot(\tilde{\rho})\csc(\tilde{\rho}_s)+(2n^2-K+3)\sec(\tilde{\rho}_s)$,

$f_5 = (\cosh(n\tilde{\rho}_s)(-f_4)+n\sinh(n\tilde{\rho}_s)f_3)$, $f_6(\tilde{\rho}_s) = (2n^2+K-3)\cos(n\tilde{\rho}_s)\sec(\tilde{\rho}_s)-n(K-1)\csc(\tilde{\rho}_s)\sin(n\tilde{\rho}_s)$,

$f_7(\tilde{\rho}_s) = n(K-1)\cos(n\tilde{\rho}_s)\csc(\tilde{\rho}_s)+(2n^2+K-3)\sec(\tilde{\rho}_s)\sin(n\tilde{\rho}_s)$,

$f_8 = (1-K)\csc(\tilde{\rho}_s)+(2n^2+K-3)\cot(\tilde{\rho})\sec(\tilde{\rho}_s)$,

$f_9 = n^2(K-1)\cot(\tilde{\rho})\csc(\tilde{\rho}_s)+(2n^2+K-3)\sec(\tilde{\rho}_s)$, $f_{10} = (\cos(n\tilde{\rho}_s)f_9+n\sin(n\tilde{\rho}_s)f_8)$,

$f_{11} = [2\tilde{\rho}\cos(2\tilde{\rho}_s)+\sin(2(\tilde{\rho}-\tilde{\rho}_s))]$, $f_{12} = (K-1)\cos(\tilde{\rho}_s)\sin(\tilde{\rho})$, $f_{13} = (\tilde{\rho}-\tilde{\rho}_s)(K-3)\sin(\tilde{\rho})$.

2. Case II: For $K > 1$, i.e., K is positive

$$p_r = \frac{C}{\kappa(1+\tilde{\rho}_1)K}\left[1-K+\frac{2(1+n^2)\cosh(\bar{\rho})[n(K-1)\cos(n\bar{\rho}-n\bar{\rho}_s)\sec h(\bar{\rho}_s)+f_{14}]}{(3-K+2n^2)\csc h(\bar{\rho}_s)f_{15}+n(K-1)\sec h(\bar{\rho}_s)f_{16}}\right], \qquad \text{Case IIa} \tag{90}$$

$$p_r = \frac{C}{\kappa(1+\tilde{\rho}_1)K}\left[1-K+\frac{2(1-n^2)[\cosh(n\bar{\rho})f_{17}(\bar{\rho}_s)-\sinh(n\bar{\rho})f_{18}(\bar{\rho}_s)]}{\sinh(n\bar{\rho})(n\sinh(n\bar{\rho}_s)f_{19}+\cosh(n\bar{\rho}_s)f_{20})+\cosh(n\bar{\rho})f_{21}}\right], \qquad \text{Case IIb} \tag{91}$$

$$p_r = \frac{C}{\kappa(1+\tilde{\rho}_1)K}\left[1-K+\frac{8\cosh(\bar{\rho})[2\bar{\rho}_s(K-1)\cosh(\bar{\rho})-4\sinh(\bar{\rho})+(K-5)\sin(\bar{\rho}-2\bar{\rho}_s)]}{8\bar{\rho}+2\bar{\rho}_s(K-1)\cosh(2\bar{\rho})-(K-5)f_{22}-4\sinh(2\bar{\rho})}\right], \qquad \text{Case IIc} \tag{92}$$

$$p_r = \frac{C(3-K)(f_{23}+\cosh(\bar{\rho})f_{24})}{\kappa(1+\tilde{\rho}_1)K[(3-K)\cosh(\bar{\rho}_s)\sinh(\bar{\rho})+\cosh(\bar{\rho})f_{24}]}, \qquad \text{Case IId} \tag{93}$$

where

$\bar{\rho} = \cosh^{-1}\sqrt{\frac{K+\tilde{\rho}_1}{K-1}}$, $\bar{\rho}_s = \cosh^{-1}\sqrt{\frac{K+\tilde{\rho}_{1s}}{K-1}}$,

$f_{14} = (-3+K-2n^2)\mathrm{csch}(\bar{\rho}_s)\sin[n(\bar{\rho}-\bar{\rho}_s)]$, $f_{15} = -\cosh(\bar{\rho})\sin(n(\bar{\rho}-\bar{\rho}_s))+n\cos(n(\bar{\rho}-\bar{\rho}_s))\sinh(\bar{\rho})$,

$f_{16} = \cos[n(\bar{\rho}-\bar{\rho}_s)]\cosh(\bar{\rho})+n\sin[n(\bar{\rho}-\bar{\rho}_s)]\sinh(\bar{\rho})$,

$f_{17}(\bar{\rho}_s) = n(K-1)\cosh(n\bar{\rho}_s)\sec h(\bar{\rho}_s)+(-3+K+2n^2)\mathrm{csch}(\bar{\rho}_s)\sinh(n\bar{\rho}_s)$,

$f_{18}(\bar{\rho}_s) = (-3+K+2n^2)\cosh(n\bar{\rho}_s)\mathrm{csch}(\bar{\rho}_s)-n(K-1)\sec h(\bar{\rho}_s)\sinh(\bar{\rho}_s)$,

$f_{19} = (1-K)\sec h(\bar{\rho}_s)+(-3+K+2n^2)\mathrm{csch}(\bar{\rho}_s)\tanh(\bar{\rho})$,

$f_{20} = (-3+K+2n^2)\mathrm{csch}(\bar{\rho}_s)+n^2(K-1)\mathrm{sech}(\bar{\rho}_s)\tanh(\bar{\rho})$,

$f_{21}(\bar{\rho}) = n\cosh(n\bar{\rho}_s)f_{19}-\sinh(n\bar{\rho}_s)f_{20}$, $f_{22} = 2\bar{\rho}\cosh(2\bar{\rho}_s)-\sinh(2(\bar{\rho}-\bar{\rho}_s))$,

$f_{23} = (K-1)\cosh(\bar{\rho}_s)\sinh(\bar{\rho})$, $f_{24} = (\bar{\rho}-\bar{\rho}_s)(K-3)\cosh(\bar{\rho}_s)+(K-1)\sinh(\bar{\rho}_s)$.

From Eqs. (86)–(93), one can observe that the radial pressure is purely density dependent, which represents the simplest theoretical form of EoS for those stars. In an argument, Dey *et al.* [100] have proposed new types of EoSs for strange matter based on a model of interquark potential. These EoSs have later been approximated to a linear function of density by Gondek-Rosinska *et al.* [102], as

$$p = a(\rho-\rho_s), \tag{94}$$

where ρ_s denotes the energy density at zero pressure, and a is non-negative constant. Such an EoS has mainly been proposed to describe the strange matter hypothesis built of u, d, and s quarks. This was done by Harko and Cheng [101], who showed that by using the Eq. (94) when $\rho_s = 4B$ ($B = 56$ MeV fm^3), the maximum mass of a strange star is $M_{\max} = 1.83\ M_\odot$.

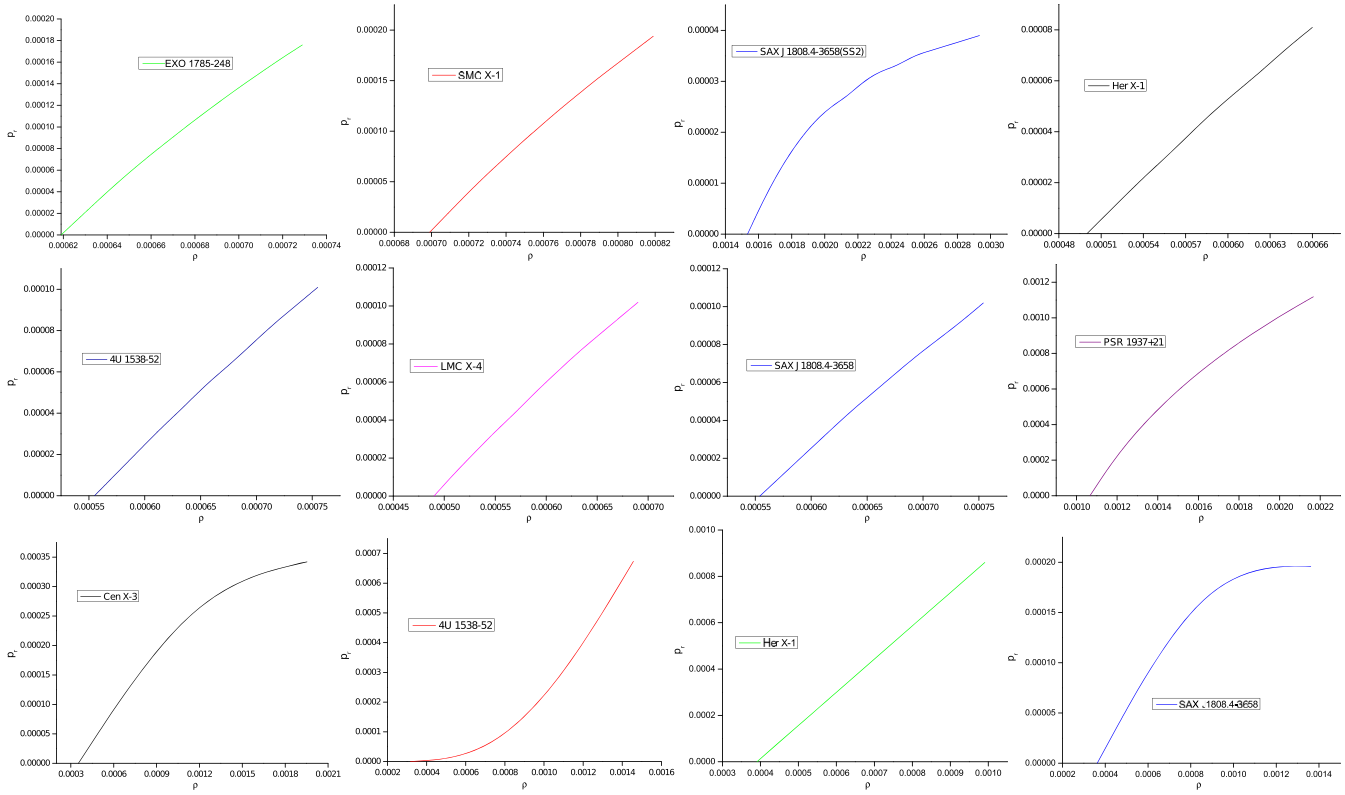

FIG. 9. Variation of radial pressure p_r (in km^{-2}) with respect to energy density ρ (in km^{-2}). For Case I, we have plotted the following stars in the first and second rows: (i) EXO 1785-248, (ii) SMC X-1, (iii) SAX J1808.4-3658(SS2)-1, and (iv) Her X-1, and (v) 4U 1538-52, (vi) LMC X-4, (vii) SAX J1808.4-3658, and (viii) PSR 1937 + 21. For Case II, we have plotted the following stars in the third row: (ix) Cen X-3, (x) 4U 1538-52, (xi) Her X-1, and (xii) SAX J1808.4-3658.

Here, we are developing our consideration the same as in [102]. In that work, authors showed that Eq. (94) corresponds to self-bound matter at the density ρ_s at zero pressure and with a fixed sound velocity. We start from a certain value of ρ_s where the pressure is zero, i.e., at the boundary for our model. The dependence of pressure on the density diagram for neutron stars with realistic EoS are represented in Fig. 9 (see Table II for considering values). For example, by the approximation of Eq. (93) in the linear power of $\rho-\rho_s$, we obtain $p_r \approx a(\rho-\rho_s)$, where $a=\frac{(3-K)}{2+\tilde{\rho}_1(1-K)^{3/2}}(1+\frac{\tilde{\rho}_1}{2K})(1+\frac{\tilde{\rho}_{1s}}{2K})$. In Fig. 9, we observe that the radial pressure p_r vanishes at surface density ρ_s. This implies that p_r can be expressed by interpolation in power of $\rho-\rho_s$. Such parametrization is very convenient for stellar modeling, which is also relevant to the interior of stable stellar configurations [102].

VI. FINAL REMARKS

In this article we have considered the Buchdahl ansatz [54] for representing a class of neutron stars in the standard framework of General Relativity. The main catch point is an extendable analytic solution for positive and negative values of spheroidal parameter K. We have focused on characterizing several exotic astrophysical objects with similar mass and radii, like LMC X-4, SMC X-1, EXO 1785-248, etc., which are confirmed by observations of gamma-ray repeaters and anomalous X-ray pulsars. To make the set of equations more tractable, we use the Gupta-Jasim [82] two-step method to solve the system of hypergeometric equations. Furthermore, pressure inside relativistic compact objects is most likely isotropic, but here we investigate the anisotropic fluid model that plays a significant role in the strong-field regime [106]. Considering the motivation, we choose anisotropy parameter Δ, which is increasing for small r, and decreasing after reaching the maximum in the interior of the star [12]. Overall, we find eight different solutions depending on the choice for the metric potential which leads to solutions of the condition of pressure anisotropy.

Based on physical requirements, we match the interior solution to an exterior vacuum Schwarzschild spacetime on the boundary surface at $r=R$, and from the comparison of both side metrics, all constants are determined which are listed in Table I. By using these constants in our investigation for several analogue objects with similar mass and radii, namely, EXO 1785-248, SMC X-1, SAX J1808.4-3658 (SS2), Her X-1, 4U 1538-52, LMC X-4, SAX J1808.4-3658,

TABLE I. Values of the model parameters of Case I and Case II for different values of K, C, n, and Δ_0.

Compact star candidates	$M(M_\odot)$	R (km)	K	CR^2	n	Δ_0	$2-K+\Delta_0 K$	Cases
EXO 1785-248 (Özel *et al.* [73])	1.3	8.849	−0.27898	0.1044	0.1	8.205	−0.01	Case Ia.
SMC X-1 (Rawls *et al.* [70])	1.04	8.301	−0.28103	0.1044	0.1	8.152	−0.01	Case Ia.
SAX J1808.4-3658 (SS2) (Li *et al.* [107])	1.3237	6.16	−1.18	0.52	1.783	0.000772	3.18	Case Ib.
Her X-1 (Abubekerov *et al.*) [75]	0.85	8.1	−1.18	0.2013		1.85	1	Case Ic.
4U 1538-52 (Rawls *et al.* [70])	0.87	7.866	−1.18	0.2145		1.85	1	Case Ic.
LMC X-4 (Rawls *et al.* [70])	1.29	8.831	−1.18	0.25006		1.85	1	Case Ic.
SAX J1808.4-3658 (Elebert *et al.* [74])	0.9	7.951	−1.18	0.2206		1.85	1	Case Ic.
PSR 1937 + 21 (Kapoor *et al.* [108], Xin *et al.*[109])	2.0833	8.04	−0.91	0.5698		3.198	0	Case Id.
Cen X-3 (Rawls *et al.* [70])	1.49	9.178	3	2.55	0.99	0.00663	−0.98	Case IIa.
4U 1538-52 (Rawls *et al.* [70])	0.87	7.866	1.78	2.915	0.4796	0.0056	0.23	Case IIb.
Her X-1 (Abubekerov *et al.*) [75]	0.85	8.1	3.1	0.8415		0.677	1	Case IIc.
SAX J1808.4-3658 (Elebert *et al.* [74])	0.9	7.951	2.1	1.759		0.048	0	Case IId.

PSR 1937 + 21, Cen X-3, 4U 1538-52, and SAX J1808.4-3658, we have studied how the anisotropy affects physical properties, such as energy density, radial, and tangential pressure. To illustrate these behaviors, we have generated a plot in Fig. 1 against the radial coordinate r/R in Km. The density and pressures are positive and remain finite at the interior of stars. Interestingly, energy density attends its maximum value at the center of stars and central densities close to the order of $\sim 10^{15}$. This bound is consistent with the argument by Ruderman [9] for anisotropic matter in certainly very high density ranges. Mainly, this situation admits the theory that the core of exotic astrophysical objects is intensely compact, particularly in the case of millisecond pulsar SAX J1808.4-3658 (SS2). We have succeeded in determining the central density of the massive pulsars 4.06×10^{15} with masses 1.3237 $M_\odot$.

To refine the model further, we have analyzed the mass-radius (M-R) relationship, generalized TOV equations, the surface redshift, energy conditions, and the EoS in linear approximation form, respectively. The obtained mass-radius ratios for anisotropic stars are consistent with Buchdahl's [54] bound, though he proposed that the isotropic object for which the energy density is non-increasing is outward from the boundary. On the other hand, based on the work by Gondek-Rosinska *et al.* [102], in which EoSs have been approximated to a linear function of density, we have plotted the dependence of pressure on the density diagram in Fig. 9, and the values used are summarized in Table II. Such an EoS is very convenient for stable stellar modeling. At the same time, we have checked the velocity of sound (v_i^2) which is less than the light's velocity as is evident in Fig. 5.

Aside from the influence on the M-R ratio for anisotropic stars, we present the variation of total mass M (normalized in solar mass $M_\odot$) with the total radius R for different chosen parametric values (see Fig. 3). We have also studied the stability of the configurations with respect to generalized TOV equation and found the equilibrium configuration

TABLE II. Energy densities, central pressure, and the Buchdahl limit for different compact star candidates for the above parameter values of Table I.

Compact star candidatesah	Central density (gm/cm^3)	Surface density (gm/cm^3)	Central pressure (dyne/cm^2)	Buchdahl condition $(2M/R \leq 8/9)$	Redshift (z_S)	Cases
EXO 1785-248	0.98×10^{15}	8.33×10^{14}	0.99×10^{35}	0.21669	0.328472	Case Ia.
SMC X-1	1.109×10^{15}	9.41×10^{14}	1.107×10^{35}	0.21546	0.325584	Case Ia.
SAX J1808.4-3658 (SS2)	4.06×10^{15}	20.65×10^{14}	1.59×10^{35}	0.3071	0.648507	Case Ib.
Her X-1	0.91×10^{15}	6.73×10^{14}	1.05×10^{35}	0.0618	0.203489	Case Ic.
4U 1538–52	1.03×10^{15}	7.47×10^{14}	1.28×10^{35}	0.16314	0.218326	Case Ic.
LMC X-4	0.95×10^{15}	6.59×10^{14}	1.45×10^{35}	0.18479	0.259444	Case Ic.
SAX J1808.4-3658	1.04×10^{15}	7.46×10^{14}	1.34×10^{35}	0.16696	0.225259	Case Ic.
PSR 1937 + 21	2.97×10^{15}	14.35×10^{14}	3.77×10^{35}	0.2692	1.049159	Case Id.
Cen X-3	3.24×10^{15}	4.76×10^{14}	5.305×10^{35}	0.23945	0.419898	Case IIa.
4U 1538-52	3.32×10^{15}	4.27×10^{14}	2.63×10^{35}	0.16314	0.643074	Case IIb.
Her X-1	1.45×10^{15}	5.27×10^{14}	1.59×10^{35}	0.15478	0.203472	Case IIc.
SAX J1808.4-3658	2.34×10^{15}	4.87×10^{14}	1.56×10^{35}	0.16696	0.225316	Case IId.

where the gravitational force (F_g) is dominating over the hydrostatic (F_h) and anisotropic (F_a) forces, as seen from Fig. 8. We conclude that our proposed model satisfies all physical requirements as well as horizon-free and stable configurations that help us further our understanding about anisotropic compact objects.

ACKNOWLEDGMENTS

S. K. M. acknowledges support from the Authority of University of Nizwa, Nizwa, Sultanate of Oman. The authors would like give special thanks to the anonymous referee for suggesting several pertinent issues which have enabled us to improve the manuscript substantially. A. P. thanks support from IUCAA, Pune, India under visiting associateship.

APPENDIX A: GUPRA-JASIM TWO-STEP METHOD

This appendix is devoted in solving the hypergeometric differential equation (HDE). Note that the HDE can be solved directly in terms of the hypergeometric series. However, some hypergeometric equations can be solved in closed form. In our preset article, we use the Gupta-Jasim [82] two-step method for solving the system of equations.

Step I: In this section, we provide the Gupta-Jasim Method in detail to supplement the results presented in the main text, starting with Eq. (10), which is

$$(1-Z^2)\frac{d^2Y}{dZ^2}+Z\frac{dY}{dZ}+(1-K+\Delta_0 K)Y=0. \tag{A1}$$

Now, differentiate the equation with respect to Z, we get

$$(1-Z^2)\frac{d^3Y}{dZ^3}-Z\frac{d^2Y}{dZ^2}+(2-K+\Delta_0 K)\frac{dY}{dZ}=0. \tag{A2}$$

Here, substitute a new variable $G=dY/dZ$, which yields

$$(1-Z^2)\frac{d^2G}{dZ^2}-Z\frac{dG}{dZ}+(2-K+\Delta_0 K)G=0. \tag{A3}$$

In the $Z<1$ case, we use the transformation $Z=\sin x$ (which corresponds the Case $K<0$, as $0<K<1$ is not a valid solution) into the Eq. (A3), and the above turns out to be (note that the first derivative term vanishes)

$$\frac{d^2G}{dx^2}+(2-K+\Delta_0 K)G=0. \tag{A4}$$

Thus we have the solution for Eq. (A4), which takes the following form:

$$\frac{dY}{dZ}=G=A_1\cosh(nx)+B_1\sinh(nx),\quad \text{where } 2-K+\Delta_0 K=-n^2. \tag{A5}$$

Step 2: In this step we find $\frac{d^2Y}{dZ^2}$ from Eq. (A5), and this yields

$$\frac{d^2Y}{dZ^2}=\frac{dG}{dZ}=\frac{dG}{dx}.\frac{dx}{dZ}=[A_1 n\sinh(nx)+B_1 n\cosh(nx)]\sec x. \tag{A6}$$

Now, inserting the expressions (A5) and (A6) into the hypergeometric Eq. (A1), and using $2-K+\Delta_0 K=-n^2$, we finally arrive at

$$Y(x)=\frac{1}{(n^2+1)}[\cosh(nx)(A_1\sin x+B_1 n\cos x)+\sinh(nx)(A_1 n\cos x+B_1\sin x)], \tag{A7}$$

which determines the $e^{\nu}=Y^2$. Similarly, one can obtain the other solutions of hypergeometric equation.

APPENDIX B: THE EXPRESSIONS FOR COEFFICIENTS USED IN EQS. (46)–(61)

We list here all the expressions that have been used to find the velocity of sound in Eqs. (46)–(61) as follows:

$N_1=\frac{4(n^2+1)\tan x}{K(1-K)\cos^2 x}\left[\frac{A_1\cosh(nx)+B_1\sinh(nx)}{\cosh(nx)(A_1+B_1 n\cot x)+\sinh(nx)(A_1 n\cot x+B_1)}\right]+\frac{2\tan x}{K\cos^2 x}+\frac{2(n^2+1)}{K(1-K)\cos^2 x}\frac{L_1}{M_1}$,

$L_1=[\cosh(nx)(A_1+B_1 n\cot x)+\sinh(nx)(A_1 n\cot x+B_1)][A_1 n\sinh(nx)+B_1 n\cosh(nx)]-[A_1\cosh(nx)+B_1\sinh(nx)]\times[n\sinh(nx)(A_1+B_1 n\cot x)-B_1\cosh(nx)n\csc^2 x+n\cosh(nx)(A_1 n\cot x+B_1)-n\sinh(nx)\csc^2 x]$,

$M_1=[\cosh(nx)(A_1+B_1 n\cot x)+\sinh(nx)(A_1 n\cot x+B_1)]^2$,

$N_2=\frac{4(1-n^2)\tan x}{K(1-K)\cos^2 x}\left[\frac{C_1\cos(nx)+D_1\sin(nx)}{C_1\cos(nx)+D_1\sin(nx)-n\cot x(C_1\sin(nx)-D_1\cos(nx))}\right]+\frac{2\tan x}{K\cos^2 x}+\frac{2(1-n^2)}{K(1-K)\cos^2 x}\frac{L_2}{M_2}$,

$L_2=[C_1\cos(nx)+D_1\sin(nx)-n\cot x(C_1\sin(nx)-D_1\cos(nx))][-nC_1\sin(nx)+D_1 n\cos(nx)]-[C_1\cos(nx)+D_1\sin(nx)][-nC_1\sin(nx)+D_1 n\cos(nx)+n\csc^2 x(C_1\sin(nx)-D_1\cos(nx))-n\cot x(C_1 n\cos(nx)+D_1 n\sin(nx))]$,

$M_2=[C_1\cos(nx)+D_1\sin(nx)-n\cot x(C_1\sin(nx)-D_1\cos(nx))]^2$.

$N_3=\frac{8(2-\cos^2 x)}{K(1-K)\cos^3 x}\left[\frac{E_1\cos(x)+F_1\sin(x)}{E_1(2x+\sin 2x)-F_1\cos 2x}\right]+\frac{2\tan x}{K\cos^2 x}+\frac{8\sin x}{K(1-K)\cos^2 x}$,

$$M_3 = \left[\frac{(E_1(2x+\sin 2x)-F_1\cos 2x)(-E_1\sin x+F_1\cos x)-(E_1\cos x+F_1\sin x)(4E_1\cos^2 x+2F_1\sin 2x)}{(E_1(2x+\sin 2x)-F_1\cos 2x)^2}\right].$$

$$N_4 = \frac{2\tan x}{K\cos^2 x}+\frac{2\sin x}{K(1-K)\cos^2 x}\left[\frac{(G_1(\cos x+x\sin x)+H_1\sin x)G_1-(G_1 x+H_1)(G_1 x\cos x+H_1\cos x)}{(G_1(\cos x+x\sin x)+H_1\sin x)^2}\right]+\frac{2(2-\cos^2 x)}{K(1-K)\cos^3 x}\left[\frac{G_1(x)+H_1}{G_1(\cos x+x\sin x)+H_1\sin x}\right].$$

$$N_5 = \frac{-4(n^2+1)\cosh x}{K(K-1)\sinh^3 x}\left[\frac{A_2\cos(nx)+B_2\sin(nx)}{A_2\cos(nx)+B_2\sin(nx)+n\tanh x(A_2\sin(nx)-B_2\cos(nx))}\right]+\frac{2\cosh x}{K\sinh^3 x}+\frac{2(n^2+1)}{K(1-K)\sinh^2 x}\frac{L_5}{M_5},$$

$$L_5 = [A_2\cos(nx)+B_2\sin(nx)+n\tanh x(A_2\sin(nx)-B_2\cos(nx))][-A_2 n\sin(nx)+B_2 n\cos(nx)]-[A_2\cos(nx)+B_2\sin(nx)][-nA_2\sin(nx)+B_2 n\cos(nx)+n\,\mathrm{sech}^2 x(A_2\sin(nx)-B_2\cos(nx))+n\tanh x(A_2 n\cos(nx)+B_2 n\sin(nx))],$$

$$M_5 = [A_2\cos(nx)+B_2\sin(nx)+n\tanh x(A_2\sin(nx)-B_2\cos(nx))]^2,$$

$$S_2 = \frac{2\cosh x\sinh^2 x(K-1)-4\cosh x(3-K+(K-1)\cosh^2 x)}{K(K-1)\sinh^5 x}.$$

$$N_6 = \frac{-4(1-n^2)\coth x}{K(K-1)\sinh^2 x}\left[\frac{C_2\cosh(nx)+D_2\sinh(nx)}{[C_2\cosh(nx)+D_2\sinh(nx)]-n\tanh x[C_2\sinh(nx)+D_2\cosh(nx)]}\right]+\frac{2\cosh x}{K\sinh^3 x}+\frac{2(1-n^2)}{K(K-1)\sinh^2 x}\frac{L_6}{M_6},$$

$$L_6 = [C_2\cosh(nx)+D_2\sinh(nx)-n\tanh x(C_2\sinh(nx)+D_2\cosh(nx))][C_2 n\sinh(nx)+D_2 n\cosh(nx)]-[C_2\cosh(nx)+D_2\sinh(nx)][nC_2\sinh(nx)+D_2 n\cosh(nx)-n\,\mathrm{sech}^2 x(C_2\sinh(nx)+D_2\cosh(nx))-n\tanh x(C_2 n\cosh(nx)+D_2 n\sinh(nx))],$$

$$M_5 = [C_2\cosh(nx)+D_2\sinh(nx)-n\tanh x(C_2\sinh(nx)+D_2\cosh(nx))]^2,$$

$$N_7 = \frac{-8(1+\cosh^2 x)}{K(K-1)\sinh^3 x}\left[\frac{E_2\cosh x+F_2\sinh x}{E_2\cosh 2x+F_2(\sinh 2x-2x)}\right]+\frac{2\cosh x}{K\sinh^3 x}+\frac{8\cosh x}{K(K-1)\sinh^2 x}M_7,$$

$$M_7 = \left[\frac{(E_2\cosh 2x+F_2(\sinh 2x-2x))(E_2\sinh x+F_2\cosh x)-(E_2\cosh x+F_2\sinh x)(2E_2\sinh 2x+2F_2(\cosh 2x-1))}{(E_2\cosh 2x+F_2(\sinh 2x-2x))^2}\right].$$

$$N_8 = \frac{2\cosh x}{K\sinh^3 x}+\frac{2\cosh x}{K(K-1)\sinh^2 x}\left[\frac{(G_2(x\cosh x-\sinh x)+H_2\cosh x)G_2-(G_2 x+H_2)(G_2 x\sinh x+H_2\sinh x)}{(G_2(x\cosh x-\sinh x)+H_2\cosh x)^2}\right]+\frac{-2(1+\cosh^2 x)}{K(K-1)\sinh^3 x}\left[\frac{G_2(x)+H_2}{G_2(x\cosh x-\sinh x)+H_2\cosh x}\right].$$

$$S_1 = \frac{2\cos^2 x\sin x(K-1)+4\sin x(3-K+(K-1)\sin^2 x)}{K(K-1)\cos^5 x},$$

$$S_2 = \frac{2\cosh x\sinh^2 x(K-1)-4\cosh x(3-K+(K-1)\cosh^2 x)}{K(K-1)\sinh^5 x}.$$

[1] J. Lattimer (2010), http://stellarcollapse.org/nsmasses.
[2] R. H. Fowler, Mon. Not. R. Astron. Soc. **87**, 114 (1926).
[3] S. Chandrasekhar, Mon. Not. R. Astron. Soc. **91**, 456 (1931).
[4] S. Chandrasekhar, Mon. Not. R. Astron. Soc. **95**, 207 (1935).
[5] G. Fodor, arXiv:gr-qc/0011040.
[6] L. Herrera and N. O. Santos, Phys. Rep. **286**, 53 (1997).
[7] J. H. Jeans, Mon. Not. R. Astron. Soc. **82**, 122 (1922).
[8] G. Lemaitre, Ann. Soc. Sci. Bruxelles A **53**, 51 (1933).
[9] R. Ruderman, Rev. Astr. Astrophys. **10**, 427 (1972).
[10] R. L. Bowers and E. P. T. Liang, Astrophys. J. **188**, 657 (1974).
[11] H. Heintzmann and W. Hillebrandt, Astron. Astrophys. **38**, 51 (1975).
[12] M. K. Mak and T. Harko, Proc. R. Soc. A **459**, 393 (2003).
[13] T. Harko and M. K. Mak, Classical Quantum Gravity **21**, 1489 (2004).
[14] T. Harko and M. K. Mak, Ann. Phys. (Amsterdam) **11**, 3 (2002).
[15] T. Harko and M. K. Mak, J. Math. Phys. (N.Y.) **43**, 4889 (2002).
[16] T. Harko and M. K. Mak, Chin. J. Astron. Astrophys. **2**, 248 (2002).
[17] M. K. Mak, N. Dobson, Jr., and T. Harko, Int. J. Mod. Phys. D **11**, 207 (2002).
[18] C. M. Chaisi and S. D. Maharaj, Gen. Relativ. Gravit. **37**, 1177 (2005).
[19] J. M. Sunzu, S. D. Maharaj, and S. Ray, Astrophys. Space Sci. **352**, 719 (2014).
[20] S. K. Maurya, Y. K. Gupta, S. Ray, and B. Dayanandan, Eur. Phys. J. C **75**, 225 (2015).
[21] S. K. Maurya, Y. K. Gupta, B. Dayanandan, M. K. Jasim, and A. Al-Jamel, Int. J. Mod. Phys. D **26**, 1750002 (2017).
[22] S. K. Maurya, A. Banerjee, and S. Hansraj, Phys. Rev. D **97**, 044022 (2018).
[23] S. K. Maurya, A. Banerjee, and Y. K. Gupta, Astrophys. Space Sci. **363**, 208 (2018).
[24] D. Deb, S. R. Chowdhury, S. Ray, F. Rahaman, and B. K. Guha, Ann. Phys. (Amsterdam) **387**, 239 (2017).
[25] M. Kalam, F. Rahaman, S. Molla, and S. M. Hossein Astrophys. Space Sci. **349**, 865 (2014).
[26] M. Kalam, F. Rahaman, S. M. Hossein, and S. Ray Eur. Phys. J. C **73**, 2409 (2013).
[27] P. Bhar, M. H. Murad, and N. Pant, Astrophys. Space Sci. **359**, 13 (2015).
[28] B. S. Ratanpal, V. O. Thomas, and D. M. Pandya, Astrophys. Space Sci. **361**, 65 (2016).
[29] P. M. Takisa and S. D. Maharaj, Astrophys. Space Sci. **361**, 262 (2016).
[30] S. Thirukkanesh and S. D. Maharaj, Classical Quantum Gravity **25**, 235001 (2008).
[31] K. Lake, Phys. Rev. D **67**, 104015 (2003).

[32] L. Herrera, J. Ospino, and A. Di Parisco, Phys. Rev. D **77**, 027502 (2008).
[33] S. K. Maurya, Y. K. Gupta, and S. Ray, Eur. Phys. J. C **77**, 360 (2017).
[34] B. V. Ivanov, Phys. Rev. D **65**, 104001 (2002).
[35] R. Sharma and S. D. Maharaj, Mon. Not. R. Astron. Soc. **375**, 1265 (2007).
[36] L. Herrera and W. Barreto, Phys. Rev. D **88**, 084022 (2013).
[37] V. Varela, F. Rahaman, S. Ray, K. Chakraborty, and M. Kalam, Phys. Rev. D **82**, 044052 (2010).
[38] B. V. Ivanov, Eur. Phys. J. C **78**, 332 (2018).
[39] A. Nasim and M. Azam, Eur. Phys. J. C **78**, 34 (2018).
[40] A. A. Isayev, Phys. Rev. D **96**, 083007 (2017).
[41] B. V. Ivanov, Eur. Phys. J. C **77**, 738 (2017).
[42] P. C. Vaidya and R. Tikekar, J. Astrophys. Astron. **3**, 325 (1982).
[43] R. Tikekar, J. Math. Phys. (N.Y.) **31**, 2454 (1990).
[44] K. Komathiraj and S. D. Maharaj, J. Math. Phys. (N.Y.) **48**, 042501 (2007).
[45] L. K. Patel and S. S. Kopper, Aust. J. Phys. **40**, 441 (1987).
[46] R. Sharma, S. Mukherjee, and S. D. Maharaj, Gen. Relativ. Gravit. **33**, 999 (2001).
[47] Y. K. Gupta and N. Kumar, Gen. Relativ. Gravit. **37**, 575 (2005).
[48] R. Finch and J. E. F. Skea, Classical Quantum Gravity **6**, 467 (1989).
[49] M. S. R. Delgaty and K. Lake, Comput. Phys. Commun. **115**, 395 (1998).
[50] L. Herrera, A. Di Prisco, J. Ospino, and E. Fuenmayor, J. Math. Phys. (N.Y.) **42**, 2129 (2001).
[51] B. C. Paul and S. Dey, Astrophys. Space Sci. **363**, 220 (2018).
[52] B. C. Paul, P. K. Chattopadhyay, and S. Karmakar, Astrophys. Space Sci. **356**, 327 (2015).
[53] S. D. Maharaj, D. K. Matondo, and P. M. Takisa, Int. J. Mod. Phys. D **26**, 1750014 (2017).
[54] H. A. Buchdahl, Phys. Rev. D **116**, 1027 (1959).
[55] J. Kumar, A. K. Prasad, S. K. Maurya, and A. Banerjee, Eur. Phys. J. C **78**, 540 (2018).
[56] J. Kumar *et al.*, arXiv:1804.01779.
[57] R. Sharma, S. Karmakar, and S. Mukherjee, Int. J. Mod. Phys. D **15**, 405 (2006).
[58] M. Oertel, M. Hempel, T. Klähn, and S. Typel, Rev. Mod. Phys. **89**, 015007 (2017).
[59] A. W. Steiner, J. M. Lattimer, and E. F. Brown, Astrophys. J. **722**, 33 (2010).
[60] F. Ozel, G. Baym, and T. Guver, Phys. Rev. D **82**, 101301 (2010).
[61] F. Ozel, Rep. Prog. Phys. **76**, 016901 (2013).
[62] T. Guver and F. Ozel, Astrophys. J. **765**, L1 (2013).
[63] P. Demorest, T. Pennucci, S. M. Ransom, M. S. E. Roberts, and J. W. T. Hessels, Nature (London) **467**, 1081 (2010).
[64] T. Ebisuzaki, Publ. Astron. Soc. Jpn. **39**, 287 (1987).
[65] E. Damen *et al.*, Astron. Astrophys. **237**, 103 (1990).
[66] J. Nättilä, A. W. Steiner, J. J. E. Kajava, V. F. Suleimanov, and J. Poutanen, Astron. Astrophys. **591**, A25 (2016).
[67] E. F. Brown, L. Bildsten, and R. E. Rutledge, Astrophys. J. **504**, L95 (1998).
[68] A. Marino, N. Degenaar, T. Di Salvo, R. Wijnands, L. Burderi, and R. Iaria, Mon. Not. R. Astron. Soc. **479**, 3634 (2018).
[69] J. Antoniadis *et al.*, Science **340**, 348 (2013).
[70] M. L. Rawls, J. A. Orosz, J. E. McClintock, M. A. P. Torres, C. D. Bailyn, and M. M. Buxton, Astrophys. J. **730**, 25 (2011).
[71] T. Munoz-Darias, J. Casares, and I. G. Martinez-Pais, Astrophys. J. **635**, 502 (2005).
[72] R. L. Kelley, J. G. Jernigan, A. Levine, L. D. Petro, and S. Rappaport, Astrophys. J. **264**, 568 (1983).
[73] F. Özel, T. Güver, and D. Psaltis, Astrophys. J. **693**, 1775 (2009).
[74] P. Elebert *et al.*, Mon. Not. R. Astron. Soc. **395**, 884 (2009).
[75] M. K. Abubekerov, E. A. Antokhina, A. M. Cherepashchuk, and V. V. Shimanskii, Astronomy Reports **52**, 379 (2008).
[76] P. C. C. Freire *et al.*, Mon. Not. R. Astron. Soc. **412**, 2763 (2011).
[77] L. Herrera, A. Di Prisco, J. Martin, J. Ospino, N. O. Santos, and O. Troconis, Phys. Rev. D **69**, 084026 (2004).
[78] L. Herrera and J. P. de Leon, J. Math. Phys. (N.Y.) **26**, 2302 (1985).
[79] M. K. Gokhroo and A. L. Mehra, Gen. Relativ. Gravit. **26**, 75 (1994).
[80] M. C. Durgapal and R. Bannerji, Phys. Rev. D **27**, 328 (1983).
[81] Y. K. Gupta and M. Kumar, Astrophys. Space Sci. **299**, 43 (2005).
[82] Y. K. Gupta and M. K. Jasim, Astrophys. Space Sci. **283**, 337 (2003).
[83] W. Israel, Nuovo Cimento B **44**, 1 (1966); **48**, 463(E) (1967).
[84] S. Karmakar, S. Mukherjee, R. Sharma, and S. D. Maharaj, Pramana **68**, 881 (2007).
[85] D. E. Barraco, V. H. Hamity, and R. J. Gleiser, Phys. Rev. D **67**, 064003 (2003).
[86] C. G. Boehmer and T. Harko, Classical Quantum Gravity **23**, 6479 (2006).
[87] L. Herrera, Phys. Lett. **165A**, 206 (1992).
[88] S. Chandrasekhar, Astrophys J. **140**, 417 (1964).
[89] W. Hillebrandt and K. O. Steinmetz, Astron. Astrophys. **53**, 283 (1976).
[90] D. Horvat, S. Ilijić, and A. Marunović, Classical Quantum Gravity **28**, 025009 (2011).
[91] H. O. Silva, C. F. B. Macedo, E. Berti, and L. C. B. Crispino, Classical Quantum Gravity **32**, 145008 (2015).
[92] D. D. Doneva and S. S. Yazadjiev, Phys. Rev. D **85**, 124023 (2012).
[93] R. Schoen and S. T. Yau, Commun. Math. Phys. **65**, 45 (1979).
[94] K. D. Olum, Phys. Rev. Lett. **81**, 3567 (1998).
[95] M. Visser, B. Bassett, and S. Liberati, arXiv:gr-qc/9810026.
[96] S. W. Hawking and G. F. R. Ellis, *The large scale structure of space-time* (Cambridge University Press, England, 1973).
[97] M. Visser, Phys. Rev. D **46**, 2445 (1992).

[98] R. C. Tolman, Phys. Rev. **55**, 364 (1939).
[99] J. R. Oppenheimer and G. M. volkoff, Phys. Rev. **55**, 374 (1939).
[100] M. Dey, I. Bombacci, J. Dey, S. Ray, and B. C. Samanta, Phys. Lett. B **438**, 123 (1998).
[101] T. Harko and K. S. Cheng, Astron. Astrophys. **385**, 947 (2002).
[102] D. Gondek-Rosinska, T. Bulik, J. L. Zdunik, E. Gourgoulhon, S. Ray, J. Dey, and M. Dey, Astron. Astrophys. **363**, 1005 (2000).
[103] P. Haensel and J. L. Zdunik, Nature (London) **340**, 617 (1989).
[104] J. A. Frieman and A. Olinto, Nature (London) **341**, 633 (1989).
[105] M. Prakash, E. Baron, and M. Prakash, Phys. Lett. B **243**, 175 (1990).
[106] G. Raposo, P. Pani, M. Bezares, C. Palenzuela, and V. Cardoso, arXiv:1811.07917.
[107] X.-D. Li, I. Bombaci, M. Dey, J. Dey, and E. P. J. van den Heuvel, Phys. Rev. Lett. **83**, 3776 (1999).
[108] R. C. Kapoor and C. S. Shukre, Astron. Astrophys. **375**, 405 (2001).
[109] XU Ren-Xin, XU Xuan-Bin, and WU Xin-Ji, Chin. Phys. Lett. **18**, 837 (2001).